Kantonsschule Olten

Maturaarbeit

Heat in Motion: Experimental, Analytical, and Simulation-Based Investigations of the One-Dimensional Heat Equation

Suvirr Malli

Class G22aB: Physics and Applications of Mathematics

Supervised by

Claude Blanc

Submission Date: January 5, 2026

Abstract

This work investigates heat diffusion in one-dimensional systems through a combined experimental, analytical, and numerical approach, with the goal of comparing idealised theoretical predictions to real experimental limitations. Two experiments were conducted using a thermally insulated aluminium rod of length 0.3 m: one involving continuous heating at a fixed boundary temperature of 110 °C, and a second examining the diffusion of a localised Gaussian temperature distribution. The temporal evolution of the temperature was recorded using eight identical surface temperature sensors positioned at intervals of 4.3 cm along the rod.

The one-dimensional heat equation was derived from energy conservation principles and solved using two analytical methods. For the first experiment, the method of separation of variables with a Fourier series expansion ($N = 1000$ modes) was applied under mixed boundary conditions. For the second experiment, a Fourier transform approach yielded a closed-form solution for Gaussian initial conditions on an effectively infinite domain. Numerical solutions were obtained using the explicit Forward Euler finite difference scheme, with stability ensured through the Courant–Friedrichs–Lewy condition. All simulations were visualised using the Manim animation library.

Comparison between analytical predictions and experimental measurements demonstrates strong qualitative agreement, reproducing key features such as heat propagation rates, profile smoothing, and modal decay behaviour. Quantitative deviations at later times are attributed to environmental heat losses and finite-geometry effects. Based on the experimental data, the thermal diffusivity of the aluminium rod was estimated as $\alpha \approx 1.9 \times 10^{-4}\,\mathrm{m^2\,s^{-1}}$, approximately twice the tabulated literature value. This discrepancy is primarily attributed to systematic errors arising from surface temperature measurements and cumulative heat losses.

Preface

From my very first year at Gymnasium, it was evident to me that my final Matura project should be firmly rooted in the natural sciences, with a particular focus on physics and mathematics. My objective was to develop a project that combined an experimental setup with a numerical simulation, both of which would be connected through analytical calculations. This guiding principle significantly influenced my search for an appropriate topic. In the course of this process, I explored several fields, including pendulum dynamics and chaos theory. My initial concept involved constructing a Foucault pendulum; however, due to its considerable size and the resulting practical limitations within the school environment, I had to abandon this idea. I subsequently considered visualising the Fourier series using a vector-based representation, which would have allowed for a more compact experimental realisation. Nevertheless, this approach proved unsatisfactory from a theoretical perspective: the derivation of the Fourier series lacks sufficient justification without reference to the heat equation and the historical and mathematical context in which Fourier originally developed this concept. As I engaged more deeply with this topic, I became increasingly drawn to the heat equation itself and the complexity of its solutions. Despite describing an everyday physical phenomenon—the diffusion of heat—it reveals rich mathematical structures and far-reaching applications across physics and engineering. This contrast between its apparent simplicity in daily life and its profound analytical depth ultimately solidified my decision to focus on this field.

I would like to express my sincere gratitude and appreciation to the following people whose support, assistance, and unique contributions made this project possible. Firstly, I would like to express my sincere gratitude to my supervisor, Mr Claude Blanc, who has provided me with great support, guidance, and motivation throughout this project. Furthermore, I would like to extend my sincere gratitude to Mr Patrick Wagner, a colleague from my table tennis club, and Mr André Keller, who both made significant contributions to the setup of my experiment and identified potential obstacles during my research. Finally, I thank my family and friends for their support and understanding throughout the various phases of this work.

In the writing of this paper, external digital tools were used for linguistic support. ChatGPT and Claude assisted with text revision, while Grammarly and DeepL Write suggested precise wording and synonyms. The outputs of these tools were strictly reviewed, adapted where necessary and approved by the author. The theoretical content, the analysis and the conclusion were developed independently by the author, and no external help was used.

Contents

1 Introduction

Heat transfer is a fundamental physical process that occurs in many everyday situations, yet its mathematical description reveals a surprising level of complexity. This contrast between intuitive physical behaviour and rigorous analytical structure serves as the central motivation for this study. The work aims to combine experimental observation with mathematical modelling in order to develop a deeper understanding of heat diffusion.

The focus of this work is the one-dimensional heat equation, which describes the temporal evolution of temperature in a solid body. Rather than treating the equation abstractly, this work investigates its qualitative predictions and examines how well they correspond to observable physical behaviour. Since heat flow itself cannot be observed directly, temperature measurements provide the crucial link between theory and experiment.

At the core of this investigation lies the question of how heat diffusion can be described mathematically and how the heat equation can be solved using different methods. The experimental measurements serve to assess the extent to which these solutions reflect real physical processes. The structure of this paper reflects this approach, beginning with the theoretical background of the heat equation, followed by experimental observations, analytical and numerical solutions, and a discussion of their agreement.

2 Research Objectives

The main objective of this project is to examine how the one-dimensional heat equation can be interpreted and to assess how accurately it describes real heat diffusion in a physical system. This objective is addressed by investigating the problem from several complementary perspectives:

- Which experimental setups are suitable for observing heat diffusion in a one-dimensional body?
- Which analytical and numerical methods can be used to solve the heat equation?
- To what extent do these solutions agree with experimentally measured temperature data?
- What insights do the different solution methods provide into the mathematical structure of the heat equation, and where can similar techniques be applied in other areas of mathematics and physics?

The central research question of this work is therefore: **How accurately does the one-dimensional heat equation describe real heat diffusion in a metal rod, and how do analytical, numerical, and experimental approaches compare in capturing this behaviour?**

3 Methodology

3.1 Approach to Answering the Research Question

The methodology of this project combines experimental investigation with analytical and numerical methods. The heat equation serves as the theoretical foundation, while experiments are used to illustrate and validate its qualitative predictions.

The framework consists of three main components. First, experiments are conducted to observe heat diffusion in a metal rod under different initial and boundary conditions. Second, the heat equation is solved analytically for idealised situations in order to understand the structure of its solutions. Third, numerical methods are used to approximate solutions, which would be implemented in cases where analytical expressions are difficult or impossible to obtain.

By comparing experimental data with analytical and numerical results, the project aims to demonstrate how abstract mathematical models can be connected to real physical systems. It also shows how different solution methods complement each other in the study of partial differential equations.

3.2 Experiment

The experimental component of this project involves heating a thin metal rod that is insulated along its length. Two configurations are investigated: heating the rod at one end and heating it locally at its centre. These setups were chosen to realise different initial and boundary conditions for the heat equation.

Careful consideration was given to the choice of materials and measurement techniques. Heat losses to the environment, insufficient insulation, and low thermal conductivity can introduce significant deviations from the idealised one-dimensional model. Minimising these effects was therefore essential in order to obtain meaningful experimental results.

3.3 Mathematical Modelling and Analysis

The mathematical description of heat diffusion arises from the principle of energy conservation and leads to a partial differential equation involving both space and time. In this study, the resulting one-dimensional heat equation is analysed and solved using several analytical techniques. While similar equations exist in higher spatial dimensions, the discussion in this paper is restricted to the one-dimensional case.

Different solution methods are presented and compared, highlighting their respective advantages and limitations.

3.4 Simulation

In addition to analytical solutions, the heat equation is investigated using numerical simulation. Since the temperature evolution is fully determined by the initial temperature distribution and the imposed boundary conditions, the system can be modelled and visualised computationally.

The simulations and visualisations were implemented in Python using the open-source library *Manim*, originally developed by Grant Sanderson, creator of the educational YouTube channel *3Blue1Brown* [1]. This library is particularly well-suited for demonstrating mathematical concepts and was used to create animations and graphical representations of heat diffusion.

3.5 Data Collection and Analysis

Temperature measurements were obtained using Dual Channel K-Type thermocouple probes, allowing the temperature at several positions along the rod to be recorded with high accuracy. Measurements were taken at fixed time intervals to capture the temporal evolution of the temperature distribution.

The collected data were processed and analysed using spreadsheet software and custom-written Python scripts. These tools were used to organise the data, generate plots, and compare experimental results with analytical and numerical predictions.

3.6 Literature Review

The most significant source that guided this research was the comprehensive book titled *Notes on Diffy Qs: Differential Equations for Engineers* [2], authored by Dr Jiří Lebl. This book was crucial for the theory behind ODEs and PDEs in general, and helped break down complex ideas into simple words, explaining solution techniques in an intuitive way. Another extremely helpful source was the book titled *Data Driven Science and Engineering* [3]. This document, which the authors Dr Steven L. Brunton and Dr J. Nathan Kutz have made open-source and can be downloaded as a PDF from their website, proved invaluable due to its detailed exploration of the Fourier Transform, as well as the Fast Fourier Transform, which will be the primary method for simulating heat diffusion. To acquire the mathematical background necessary to fully understand the solution process of the heat equation, a range of educational resources were consulted, including lecture videos by the already mentioned Dr Steven L. Brunton [4] and Dr Tom Crawford [5]. These sources provided intuitive explanations of general solution techniques and are therefore not cited explicitly. Since the paper will only contain the most important steps of the calculations, the appendix will be referenced whenever needed.

Basic definitions of terminology and laws will be directly quoted from Wikipedia, while more complex ideas will be sourced from topic-specific books.

4 Theoretical foundations

Thermodynamics is a branch of physics that studies heat, temperature and work, and examines how these quantities are connected to energy transformations and the properties of physical systems. [6]. This section introduces the physical laws governing heat transfer and shows how they lead to mathematical models such as the heat equation. It contains the Zeroth and First Laws of Thermodynamics, Fourier's Law of Heat Conduction, as well as Newton's Law of Cooling, along with a detailed exploration of differential equations.

4.1 Laws of thermodynamics

4.1.1 Zeroth Law of Thermodynamics

This law states the following:

"If two systems are in thermal equilibrium with a third system, then they are in thermal equilibrium with each other" [7, p. 73].

Thermal equilibrium means that no net heat flows between systems when they are brought into contact [8]. This law is necessary for the definition of temperature scales: A thermometer (system C) is placed into a system (system A) of a certain temperature until they reach thermal equilibrium. When the thermometer is placed into a different volume (system B), and it shows the same reading as before at the thermal equilibrium point, this means that system A and system B would also be in thermal equilibrium when they come into contact (they are at the same temperature). This also shows the importance of calibration of thermometers before being used.

4.1.2 First Law of Thermodynamics

This law states the conservation of energy. Since energy cannot be created or destroyed, the internal energy of a system can only be transformed from one form to another [9]. Formulated in mathematical terms, this law can be written as:

$$\Delta U = Q + W \tag{1}$$

ΔU = change in system's internal energy $[J]$
Q = (heat) energy transferred into the system $[J]$
W = Work done on the system $[J]$

This implies that energy added to a system as heat or work must equal the change in its internal energy. Essentially, any energy change in a system results from the exchange of heat or work with its surroundings, thereby linking internal energy, heat, and work.

4.2 Thermal Conduction

4.2.1 Fourier's Law of Heat Conduction

Fourier's law states that heat flow through a material is proportional to the temperature gradient and the cross-sectional area perpendicular to the flow direction. [10]. It follows that within a

solid body, heat always flows against its gradient, so from hot to cold. As a formula, this can be described in a differential form:

$$q = -k\nabla T \tag{2}$$

q = amount of heat energy flowing per unit area per unit time $[W/m^2]$
k = measures how well a material conducts heat $[\frac{W}{m \cdot K}]$
∇T = how fast temperature changes at a certain point in space $[K/m]$

Note that the negative sign in the formula indicates that the heat flux is against the temperature gradient. This relation will be useful for the derivation of the heat Equation.

4.2.2 Newton's Law of Cooling

In the study of heat transfer, Newton's law of cooling states that the rate of heat exchange between a body and its surroundings is proportional to their temperature difference [11]. This implies that objects at a higher temperature cool more rapidly at first, while the cooling process slows down as the temperature approaches that of the environment, which is consistent with everyday experience. Mathematically, this relationship can be expressed as:

$$q = h\,(T(t) - T_{\text{env}}) = h\,\Delta T(t)$$

q = heat flux transferred from the body to the environment [W/m^2]
h = heat transfer coefficient [W/(m^2 K)]
$T(t)$ = temperature of the object's surface [K]
T_{env} = temperature of the environment [K]
$\Delta T(t)$ = time-dependent temperature difference between the body and the environment [K]

In practical situations, heat conduction within a solid body is generally accompanied by heat exchange with the surrounding environment. Newton's law of cooling is therefore commonly used to formulate realistic boundary conditions for the heat equation. Even though this law is not explicitly included in the heat equation, its effects appear as deviations from the ideal model later on in the experiment.

4.3 Differential Equations

In mathematics, a differential equation is an equation containing one or more unknown functions and their derivatives [12]. Ordinary Differential Equations (ODEs) are equations of only one independent variable, where derivatives are only with respect to this one variable. Equations with several independent variables are called partial differential equations or PDEs [2, p. 17]. While solving algebraic equations typically involves finding one or more numerical values that satisfy the equation, solving differential equations requires determining an unknown function (or a family of functions). In contrast to algebraic equations, whose solutions can often be expressed explicitly, differential equations cannot always be solved in closed form. In such cases, the solution may be given implicitly as an equation that no longer contains derivatives. Alternatively, it may be approximated using numerical methods, which are explored in Section 6.4. This distinction is particularly relevant in the context of the heat equation, since exact analytical solutions exist only for certain idealised cases, whereas more complex situations require numerical approaches.

4.3.1 Ordinary Differential Equations (ODE)

The focus now shifts to ordinary differential equations (ODEs), in which the unknown function depends on a single independent variable. Studying ODEs provides the necessary foundation for understanding solution techniques that can later be extended to partial differential equations, including the heat equation. Key concepts such as order and linearity, as well as an analytical and a numerical solution method, are presented in this section.

Order of an ODE A key criterion for classifying an ODE is its *order*, which corresponds to the highest derivative present in the equation [2, p. 17]. The significance of the order will be discussed later on.

For example, the differential equation for the population growth model

$$\frac{dy}{dt} = ky \tag{3}$$

is a first-order ODE, while the differential equation describing the motion of an object thrown upward (neglecting air resistance)

$$m\frac{d^2y}{dt^2} = -mg$$

is a second-order ODE. Most physical functions depend on a temporal variable, while functions in general are of the form $f(x)$. Lower-order equations tend to be easier to analyse and behave more simply. [2, p. 18].

Linearity Ordinary differential equations can also be classified based on how the dependent variable and its derivatives appear. An ODE is called *linear* if the dependent variable and its derivatives appear only to the first power, are not multiplied by each other, and are not inside other functions; otherwise, it is *nonlinear*.

A linear ODE of order n can be written as

$$a_n(x)\frac{d^ny}{dx^n} + a_{n-1}(x)\frac{d^{n-1}y}{dx^{n-1}} + \cdots + a_1(x)\frac{dy}{dx} + a_0(x)y = b(x),$$

with $a_0, \ldots, a_n$ being *coefficients*, which may depend arbitrarily on the independent variable x [2, p. 18].

For example,

$$e^x \frac{d^2y}{dx^2} + \sin(x)\frac{dy}{dx} + x^2 y = \frac{1}{x}$$

is linear, as y and its derivatives appear only linearly.

In contrast,

$$\frac{dx}{dt} = x^2$$

is a first-order *nonlinear* ODE, since the dependent variable x appears to the second power [2, p. 19]. This property of linearity will be particularly important when applying the method of separation of variables later on, as it allows the dependent variable and its derivatives to be treated independently.

Separation of variables and Initial Conditions One of the standard techniques for solving linear ordinary differential equations is the method of *separation of variables*, in which the variables are separated, allowing each side of the equation to depend on only one variable and be integrated independently. This method will later be extended to partial differential equations.

A differential equation is *separable* if it can be written as

$$\frac{dy}{dx} = f(x)g(y).$$

To solve this, all terms depending on x can be moved to one side, while all terms depending on y are moved to the other. The equation can be rewritten as

$$\frac{1}{g(y)}\,dy = f(x)\,dx.$$

Integrating both sides gives

$$\int \frac{1}{g(y)}\,dy = \int f(x)\,dx + C.$$

which can be solved for y, if closed-form expressions for the two integrals can be found [2, p. 33]. This suggests why differential equations do not always have closed-form solutions. To determine the constants arising from integration, so-called *initial conditions* are required. An initial condition specifies the value of the function or one of its derivatives at a particular point. In general, n initial conditions are needed to determine a unique solution for an n-th-order ODE.

Exponential Solutions Many physical systems lead to differential equations whose solutions are exponential functions. To illustrate this behaviour, a representative differential equation is considered, which is representative of equations arising in physical contexts such as the heat equation:

$$\frac{dT}{dt} = -\lambda T. \tag{4}$$

Here, the symbol $T(t)$ denotes a purely temporal function. It should not be confused with the temperature field $u(x,t)$ introduced later in the heat equation. The equation presented is of the same type as the population growth model (3), with the difference that in this case the solution is an exponentially decaying function due to the negative factor $-\lambda$. Nevertheless, both equations can be solved using the method of separation of variables, since they are linear ordinary differential equations.

As discussed earlier, all terms involving T can be moved to one side of the equation, while all terms involving t are moved to the other. Integrating both sides yields

$$\int \frac{1}{T}\,dT = \int -\lambda\,dt + C.$$

Evaluating the integrals gives

$$\ln|T| = -\lambda t + C.$$

Exponentiating both sides yields

$$|T| = e^{-\lambda t + C} = e^{C} e^{-\lambda t}.$$

Since e^C is a positive constant, it can be replaced by a new constant $D > 0$. Removing the absolute value then gives the general solution

$$T(t) = De^{-\lambda t}.$$

If an initial condition $T(0) = T_0$ is given, the constant D can be determined uniquely. Substituting $t = 0$ yields

$$T_0 = D,$$

and thus the solution takes the form

$$T(t) = T_0 e^{-\lambda t}. \tag{5}$$

Interpreting this solution, the rate of change of $T(t)$ is proportional to its current value at any point in time, which leads to an exponential decay. The constant T_0 represents the scaling factor of the solution and ensures that the initial condition $T(0) = T_0$ is satisfied.

Numerical Approximation: The Forward Euler Method While separation of variables provides exact analytical solutions for many ordinary differential equations, numerical methods offer an alternative approach that approximates solutions through discretisation. The *Forward Euler method*, also known as Euler's method, introduces fundamental concepts that extend to partial differential equations and will be used analysed and used in Section 6.4.

The method is based on approximating the derivative using a forward difference formula. Consider a first-order ODE of the form

$$\frac{dy}{dt} = f(t, y), \quad y(t_0) = y_0.$$

The time domain is discretized into equally spaced points $t_n = t_0 + n\Delta t$, where Δt is the time step and $n = 0, 1, 2, \ldots$ The derivative at time t_n can be approximated using the definition of the derivative:

$$\left.\frac{dy}{dt}\right|_{t=t_n} \approx \frac{y(t_{n+1}) - y(t_n)}{\Delta t}.$$

Substituting this approximation into the differential equation and denoting $y_n \approx y(t_n)$ yields the Forward Euler update formula [2, p. 57]:

$$y_{n+1} = y_n + \Delta t\, f(t_n, y_n). \tag{6}$$

This explicit scheme computes the solution at the next time step t_{n+1} directly from the current state at t_n, making it straightforward to implement.

As an example, applying the Forward Euler method to the exponential decay equation (4) gives

$$T_{n+1} = T_n + \Delta t\,(-\lambda T_n) = (1 - \lambda\Delta t)T_n.$$

Starting from the initial condition T_0, successive iterations yield

$$T_n = (1 - \lambda\Delta t)^n T_0.$$

For sufficiently small time steps, this discrete solution approximates the exact exponential solution $T(t) = T_0 e^{-\lambda t}$, since $(1 - \lambda\Delta t)^n \approx e^{-\lambda n \Delta t} = e^{-\lambda t_n}$ as $\Delta t \to 0$.

The accuracy of the Forward Euler method depends on the time step size. The *local truncation error*—the error introduced in a single time step—is proportional to $(\Delta t)^2$, making the method first-order accurate in time [2, p. 58]. Smaller time steps yield more accurate solutions but require more computational steps. Additionally, the method is only conditionally stable: the time step must be chosen carefully to prevent numerical instabilities that cause the solution to grow unboundedly.

The Forward Euler scheme extends naturally to systems of ordinary differential equations and, more importantly, to partial differential equations by discretising both space and time. This extension forms the basis of finite difference methods for solving the heat equation, as will be discussed in Section 6.4. The concepts of discretisation, stability conditions, and the balance between accuracy and computational cost introduced here remain central to numerical solutions of partial differential equations.

4.3.2 Partial Differential Equations (PDE)

The methods introduced for ordinary differential equations form the foundation for solving more complex equations arising in physics. In many physical problems, however, the quantity of interest depends on more than one independent variable, such as both space and time. This leads to partial differential equations, which generalise ordinary differential equations and require adapted solution techniques. Even though PDEs differ significantly from ODEs, the concepts of order and linearity still apply.

The method of separation of variables can only be applied under specific conditions. The partial differential equation must be linear and homogeneous, meaning that all terms depend on the dependent variable [2, p. 19], and the boundary conditions must be independent of time. Furthermore, the spatial domain must be fixed and separable, and it must be possible to express the solution as a product of functions, each depending on a single independent variable. Under these assumptions, the principle of superposition applies, and the full solution can be constructed as a sum of separated solutions. The one-dimensional heat equation with constant material parameters satisfies all these conditions, making it particularly well-suited for this method.

Principle of Superposition If a differential equation is linear, it satisfies the principle of superposition. This means that if u_1 and u_2 are solutions of a homogeneous linear equation, then any linear combination

$$u_3 = c_1 u_1 + c_2 u_2$$

with constants c_1 and c_2 is also a solution [2, p. 137]. This property is essential for the heat equation, as it allows the full solution to be constructed by adding separated solutions corresponding to different spatial modes, each evolving independently in time.

The Heat Equation Consider a wire of length L, insulated along its length except at the endpoints. Let x denote the position along the wire and t denote time.

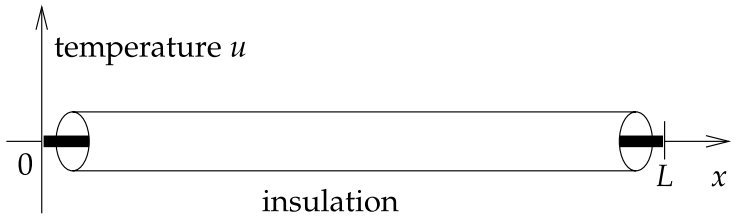

Figure 1: Schematic of a thin metal rod of length L, showing the spatial coordinate x and boundary temperatures at the endpoints. [2, p. 232]

The temperature at position x and time t is denoted by $u(x,t)$. The evolution of the temperature along the wire is described by the one-dimensional heat equation,

$$\frac{\partial u}{\partial t} = \alpha \frac{\partial^2 u}{\partial x^2}, \tag{7}$$

where $\alpha > 0$ is the thermal diffusivity of the material [2, p. 232]. The transient process of heat conduction, described by a PDE, was first formulated by Jean Baptiste Joseph Fourier (1768-1830) and presented as a manuscript to the Institut de France in 1807 [13, p. 151].

PDEs are often written using subscript notation rather than differential quotients. The subscript indicates the variable with respect to which differentiation is performed, and repeated subscripts indicate higher-order derivatives. Rewriting the heat equation in this way gives

$$u_t = \alpha\, u_{xx},$$

where u_t denotes the partial derivative of u with respect to time, and u_{xx} denotes the second partial derivative with respect to the spatial coordinate x.

The heat equation is physically intuitive: at each point along the rod, the rate of change of temperature is proportional to the curvature of the temperature profile. Regions of local maximum temperature decrease over time, while regions of local minimum temperature increase, reflecting the natural flow of heat from hotter to colder areas. This linear second-order partial differential equation constitutes the central focus of this paper and will be analysed using both analytical and numerical methods in the following sections.

Separation of Variables Unlike the ODE (4), the heat equation involves two independent variables. The method of separation of variables, therefore, requires an additional assumption. First, the function $u(x,t)$ is written as a product of two functions, one depending only on time and one depending only on space. The following assumption is made:

$$u(x,t) = X(x)T(t). \tag{8}$$

If such a representation exists, the heat equation can be formulated as

$$X(x)T'(t) = \alpha X''(x)T(t).$$

by substituting $u(x,t) = X(x)T(t)$ into the heat equation. This representation of the derivative makes the following steps easier to follow. Isolating X and its second derivative on one side gives

$$\frac{T'(t)}{\alpha T(t)} = \frac{X''(x)}{X(x)}.$$

This equation must hold for all x and all t. However, the left-hand side depends only on t, while the right-hand side depends only on x. Hence, each side must be a constant. This constant can

be called $-\lambda$ (the minus sign is chosen so that physically relevant solutions decay in time). The following two (uncoupled) equations are obtained:

$$\begin{aligned} X''(x) + \lambda X(x) &= 0, \\ T'(t) + \lambda \alpha T(t) &= 0. \end{aligned} \tag{9}$$

These linear differential equations can now be solved; both often arise in other fields of physics, too, the first being the differential equation with oscillating functions as solutions, and the second having exponentially decaying functions as solutions. This equation is of the same type as (4), which was solved earlier. This analytical approach was applied by Fourier himself [13, p. 155] and will be discussed further in the calculation section (see Section 6.2.1).

Initial and Boundary Conditions Solving the heat equation requires both initial and boundary conditions. Since the equation involves one first-order derivative in time and one second-order derivative in space, one initial condition in time and two boundary conditions in space are required.

Because the spatial variable x is defined on the interval $[0, L]$, the boundary conditions are typically prescribed at the endpoints. Common choices are Dirichlet boundary conditions,

$$u(0,t) = a \quad \text{and} \quad u(L,t) = b,$$

, Neumann boundary conditions,

$$u_x(0,t) = a \quad \text{and} \quad u_x(L,t) = b,$$

or Mixed (Dirichlet-Neumann) boundary conditions

$$u(0,t) = a \quad \text{and} \quad u_x(L,t) = b,$$

where a and b are constants.

The initial condition specifies the temperature distribution at time $t = 0$ and is given by

$$u(x,0) = f(x),$$

where $f(x)$ is a given function. The solution $u(x,t)$ must satisfy all initial and boundary conditions simultaneously. Various combinations of the boundary conditions will be analysed in the calculation section.

Solution by Integral Transforms Besides separation of variables, partial differential equations can also be solved using integral transform methods. The basic idea is to transform the original equation into a different mathematical domain in which derivatives become algebraic expressions. This often simplifies the equation and allows it to be solved more easily.

For the heat equation, the most important example is the Fourier transform. Applying the Fourier transform with respect to the spatial variable converts the heat equation into an ordinary differential equation in time for each frequency component. These resulting equations can be solved using standard methods for ordinary differential equations. The solution in physical space is then obtained by applying the inverse transform. Transform methods are particularly useful for problems defined on infinite or semi-infinite domains and will be used in Section 6.2.3 to solve the heat equation in an alternative way besides the separation of variables.

5 Experiment

5.1 Setup

To obtain an empirical understanding of the temperature evolution predicted by the heat equation, an experiment was conducted to observe thermal diffusion along a solid body subjected to a controlled heat source. The experimental arrangement closely resembles the classical physical configuration from which the one-dimensional heat equation is derived: a thin, insulated metal rod heated at one end, as illustrated in Figure 2.

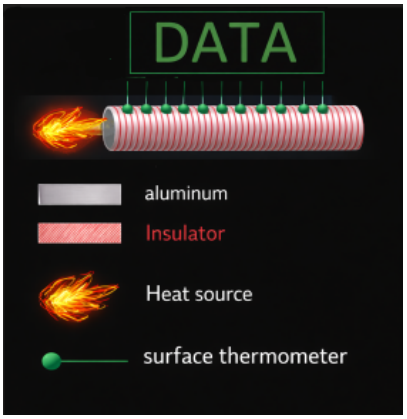

Figure 2: Schematic of the experimental setup. [Author's Own]

Although the underlying concept is straightforward, its experimental realisation poses several practical challenges. The selection of materials and measurement equipment is critical, as parameters such as rod diameter, insulation quality, and temperature sensor characteristics strongly influence the observed heat transfer behaviour. To address these challenges, several experimental arrangements were tested. The goal was to identify a setup that closely approximates one-dimensional heat conduction while yielding reliable and reproducible data.

The initial arrangement employed an aluminium rod with a diameter of 4 cm and a length of 0.3 m. Most of the rod was insulated using fibreglass wool, while one end remained exposed to act as the heating interface. Thermal energy was supplied by a basic heating plate similar to a hotplate. The temperature distribution along the rod was monitored using eight sensors positioned at evenly spaced locations on the surface, with the first sensor placed directly adjacent to the heat source and the final sensor located at the opposite end of the rod. Since drilling into the rod was not feasible, surface measurements were required. Dual-channel K-type thermocouple probes were used, providing accurate and reliable temperature readings at each measurement point.

Despite its close resemblance to the intended theoretical design, this configuration produced results that deviated from expectations. The temperature within the rod increased only slowly, and the sensor closest to the heat source exhibited pronounced temporal fluctuations.

Further investigation revealed that these fluctuations originated from the thermostat mechanism of the heating plate. Many simple heating devices operate with a temperature hysteresis, meaning that heating is switched on and off within a predefined temperature interval rather than being regulated continuously. This behaviour results in periodic variations in the supplied heat flux [14]. Since the objective was to analyse heat conduction under temporally stable boundary conditions, this type of heat source proved unsuitable.

A heating device with manually adjustable, stable temperature control was subsequently obtained from Lumatron AG, thereby eliminating fluctuations in the boundary condition. The slow temperature increase observed in the initial arrangement was attributed primarily to the large diameter of the rod. Its substantial thickness increased the thermal mass and allowed for significant heat transport in directions perpendicular to the rod axis, violating the assumption of one-dimensional heat flow. This limitation was addressed by replacing the rod with one of smaller diameter, substantially improving the validity of the one-dimensional approximation. Figure 3 shows the final experimental arrangement.

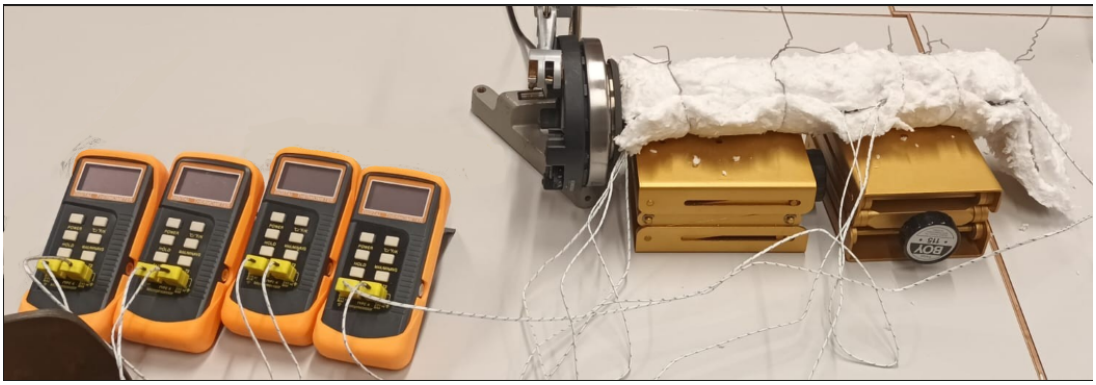

Figure 3: Photograph of the experimental setup used to measure heat propagation along the aluminium rod. [Author's Own]

These observations underline the importance of carefully controlling experimental parameters when modelling physical systems using partial differential equations. The refined setup formed the basis for all measurements analysed in the subsequent sections.

5.2 Choice of Initial and Boundary Conditions

To enable a meaningful comparison between experimental measurements and solutions of the one-dimensional heat equation, the physical system is idealised as a homogeneous rod with constant material properties and predominantly one-dimensional heat conduction. Under these assumptions, appropriate initial and boundary conditions must be specified for each experimental configuration, as discussed earlier in Section 4.3.2. In the present context, these conditions are determined by the experimental arrangement and by the thermal state of the rod at the beginning of each measurement.

In the first experiment, heat was supplied continuously at the left end of the rod by a heating plate maintained at an approximately constant temperature of 110°C. This situation is described by a fixed-temperature (Dirichlet) boundary condition at $x = 0$. The right end of the rod was thermally insulated, corresponding to an approximately zero heat flux (Neumann) boundary condition at $x = 0.3$. At the start of the measurement, the temperature distribution along the rod was nearly uniform and close to the ambient room temperature of 22°C, which serves as the initial condition for the heat equation.

In the second experiment, heat was applied for a short time period locally near the centre of the rod, causing a higher temperature in the middle of the rod. Data acquisition began after the heat had already partially diffused, resulting in a smooth and nearly symmetric temperature profile with a maximum near the centre. This initial temperature distribution can be well approximated by a Gaussian function. Both ends of the rod were insulated, leading to approximately zero heat flux boundary conditions at $x = 0$ and $x = 0.3$. Although the thermal insulation was improved compared to the first experiment, some heat loss to the surrounding air remained unavoidable and is reflected in the gradual decrease of the average temperature over time.

5.3 Experimental Results

The experimentally measured temperature data for both configurations are presented below. The results are visualised using time–temperature plots for individual sensors, which are spaced approximately 4.3 cm apart. This spatial resolution allows the temporal evolution of heat propagation along the rod to be examined in detail. Complete numerical datasets for all sensors and

time steps are provided in Appendix A.

5.3.1 Experiment 1: Heating at One End

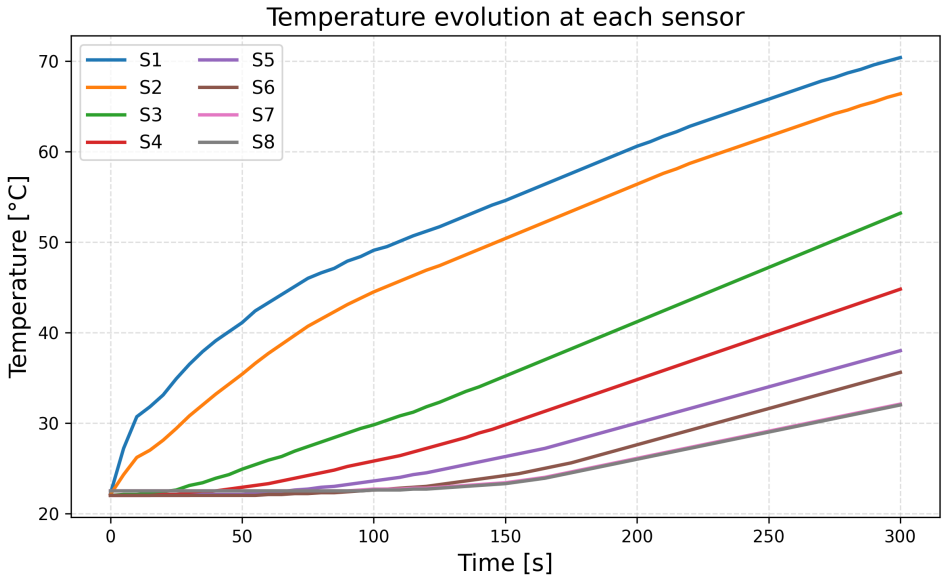

Figure 4: Measured temperature as a function of time for selected sensor positions in Experiment 1. [Author's Own]

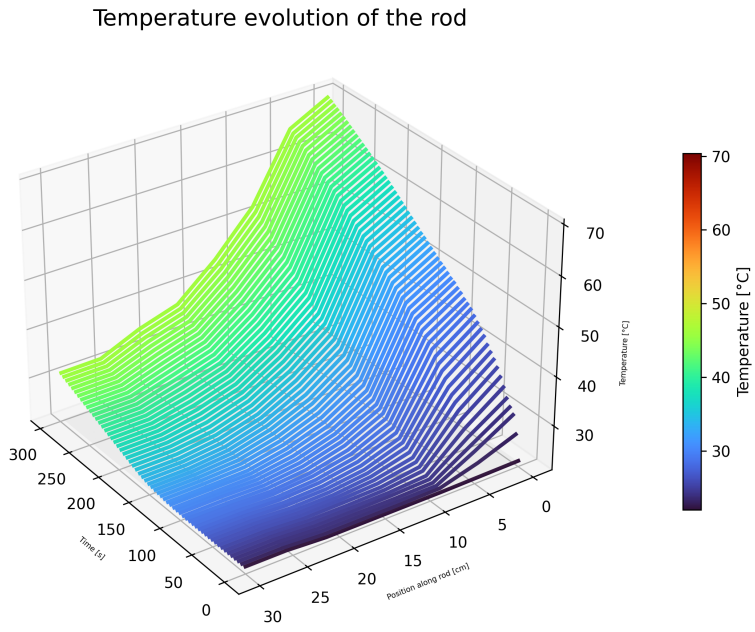

Figure 5: Measured spatio-temporal evolution of the temperature along the rod in Experiment 1. [Author's Own]

5.3.2 Experiment 2: Diffusion from a Localised Temperature Peak

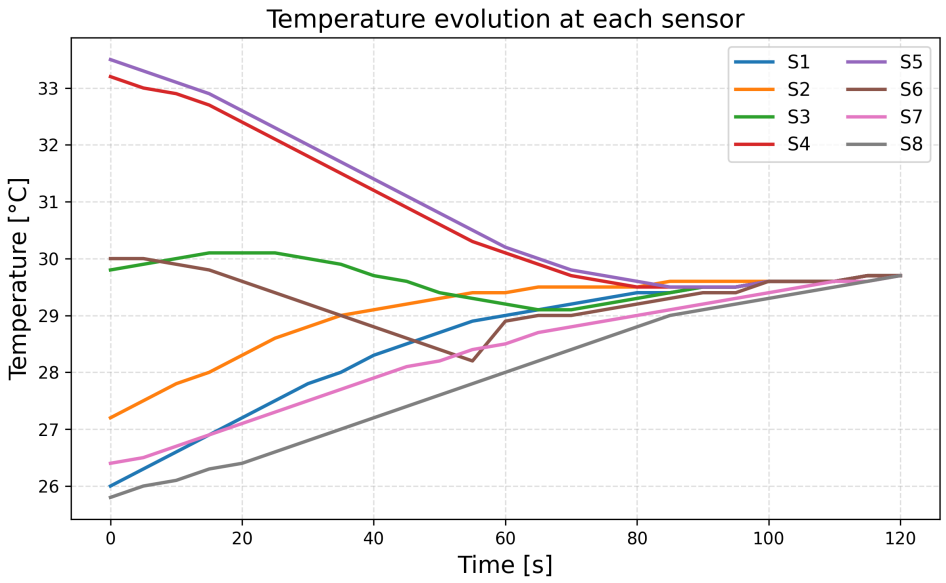

Figure 6: Measured temperature as a function of time for selected sensor positions in Experiment 2. [Author's Own]

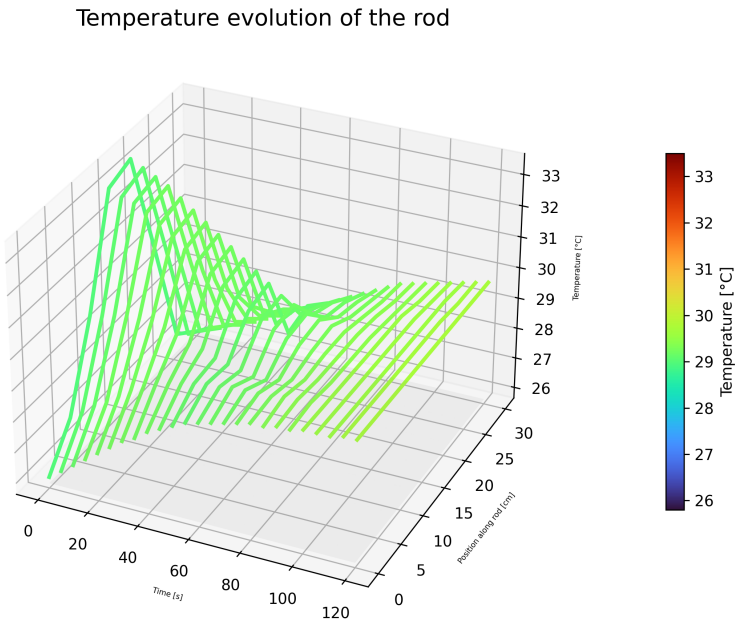

Figure 7: Measured spatio-temporal evolution of the temperature along the rod in Experiment 2. [Author's Own]

5.4 Discussion of the Experimental Results

5.4.1 Experiment 1

The first experiment investigates heat propagation along the rod under continuous heating at one end. Sensor S1, positioned closest to the heat source, exhibits a rapid initial temperature

increase and gradually approaches the imposed boundary temperature of 110°C. In contrast, sensor S8 at the opposite end of the rod displays a clear temporal delay before its temperature begins to rise, reflecting the finite time required for thermal diffusion.

The intermediate sensors S2 to S7 exhibit behaviour that smoothly interpolates between these two limiting cases. With increasing distance from the heat source, the onset of temperature increase is progressively delayed and the rate of change decreases, as shown in Figure 4. The three-dimensional representation in Figure 5 illustrates the gradual propagation of the thermal front and the smoothing of the temperature profile over time.

Overall, the monotonic temperature increase observed at all sensor positions, together with the decreasing temporal gradients, is fully consistent with the qualitative predictions of the one-dimensional heat equation subject to a fixed-temperature boundary condition.

5.4.2 Experiment 2

The second experiment examines the evolution of an initially localised temperature distribution without continuous external heating. At the start of the measurement, a pronounced temperature maximum of approximately 33.5°C is observed near the centre of the rod (sensor S4), while sensors farther from the centre record temperatures close to ambient conditions.

As time progresses, the temperature at S4 decreases as thermal energy diffuses away from the initially heated region. Adjacent sensors S3 and S5 show a delayed increase in temperature before also beginning to cool, as illustrated in Figure 6. Sensors farther from the centre respond at later times, demonstrating the gradual redistribution of heat along the rod.

The three-dimensional representation in Figure 7 highlights the progressive flattening of the initially peaked temperature profile. As spatial temperature gradients decrease, the temporal rate of change diminishes, and the temperature curves converge. In contrast to Experiment 1, the temperature evolution is non-monotonic, and the average temperature decreases over time due to heat losses to the surrounding air.

5.4.3 Comparison of Experiments 1 and 2

The contrasting behaviour observed in the two experiments arises primarily from the different initial and boundary conditions. In Experiment 1, thermal energy is continuously supplied at one end of the rod, leading to a monotonic temperature increase at all sensor positions. Although a steady state is not reached within the measurement period, the heat equation predicts that, after sufficiently long times, the rod would approach a uniform temperature equal to the imposed boundary temperature of 110°C.

In Experiment 2, no external heat is added after the initial heating. The temperature evolution, therefore, is governed by internal heat redistribution and unavoidable losses to the surrounding air. This results in a gradual decrease of the average temperature and convergence toward a uniform profile determined by the initial thermal energy of the system.

5.4.4 Calculation of Thermal Diffusivity

Beyond qualitative agreement between experiment and theory, the measured data allow an estimate of the thermal diffusivity of the aluminium rod to be obtained. The thermal diffusivity α is a material parameter appearing in the one-dimensional heat equation (7) and quantifies the rate at which heat propagates within a material [15].

Starting from

$$u_t = \alpha u_{xx},$$

the thermal diffusivity can formally be written as

$$\alpha = \frac{u_t}{u_{xx}}.$$

However, this expression is unsuitable for direct experimental evaluation, as the required partial derivatives cannot be determined reliably from discrete and noisy measurement data.

Instead, the heat equation is interpreted in terms of characteristic spatial and temporal scales. Dimensional analysis of the equation yields the scaling relation

$$\alpha \sim \frac{L^2}{t}, \tag{10}$$

where L denotes a characteristic distance along the rod and t a characteristic diffusion time. This relation implicitly assumes a semi-infinite geometry and negligible boundary effects during the relevant time interval. Although it is exact only up to a dimensionless factor that depends on the specific initial and boundary conditions, it provides a robust order-of-magnitude estimate and correctly reflects the physical interpretation of thermal diffusivity.

The first experiment is particularly well-suited to this approach because of the presence of a well-defined thermal front. For each sensor, the characteristic time t is defined as the moment at which the local temperature exceeds its initial value by a fixed threshold of $\Delta T = 6°\mathrm{C}$. This choice represents a compromise: smaller thresholds are dominated by early-time transients and surface effects, while larger thresholds increasingly amplify the influence of heat losses. Since the maximum temperature rise at the farthest sensor is approximately 9.5°C, a threshold of $\Delta T = 6°\mathrm{C}$ remains sufficiently below the maximum while shifting the estimation towards later times, where diffusive behaviour dominates.

The corresponding distance x is taken as the sensor position relative to the heated boundary. Using the scaling relation (10), an individual estimate of α is obtained for each sensor. Sensor S1 is excluded, as it is located directly at the boundary and does not exhibit a measurable diffusion delay.

Table 1: Estimation of the thermal diffusivity α from Experiment 1 using a 6°C temperature rise criterion.

Sensor	Distance x (m)	Time t (s)	$\alpha = \frac{x^2}{t}$ ($\mathrm{m^2\,s^{-1}}$)
S2	0.043	20	9.3×10^{-5}
S3	0.086	70	1.1×10^{-4}
S4	0.129	125	1.3×10^{-4}
S5	0.171	170	1.7×10^{-4}
S6	0.214	205	2.2×10^{-4}
S7	0.257	235	2.8×10^{-4}
S8	0.300	265	3.4×10^{-4}

Averaging over sensors S2 to S8 yields

$$\alpha_{\mathrm{mean}} \approx 1.9 \times 10^{-4}\,\mathrm{m^2\,s^{-1}}.$$

This value exceeds the tabulated thermal diffusivity of aluminium at room temperature ($\alpha \approx 9.7 \times 10^{-5}\,\mathrm{m^2\,s^{-1}}$ [15]) by a factor of ~ 2. The systematic increase of the estimated diffusivity with

distance can be interpreted as a consequence of several factors. These include the oversensitivity of the sensors to temperature changes, the inevitable imprecision in their positioning and the limited validity of the scaling relation due to the finite rod thickness. Together, these effects accelerate the apparent arrival of the thermal front at larger distances and thereby bias the diffusivity estimate.

Despite these limitations, the order of magnitude and overall consistency of the estimated values support the validity of modelling the observed temperature evolution using the one-dimensional heat equation.

6 Mathematical Modelling and Analysis

Having established the physical interpretation and theoretical background of the heat equation in Section 4, the focus now shifts to a detailed mathematical analysis. Rather than repeating the general theory of partial differential equations and boundary conditions presented earlier, this section concentrates on the explicit derivation of the one-dimensional heat equation and the analytical and numerical methods used to solve it under idealised assumptions.

The two experiments conducted differ fundamentally in their initial and boundary conditions, making each particularly well-suited to a different solution approach. Experiment 1, which involves continuous heating at one end of the rod with fixed boundary conditions, is naturally addressed using the method of separation of variables combined with Fourier series. Experiment 2, featuring a localised Gaussian temperature peak that diffuses without external heating, is ideally suited for a Fourier transform solution on an effectively infinite domain. Both analytical approaches will be complemented by numerical methods that can handle more general situations.

6.1 Derivation of the Heat Equation

The formulation and application of the one-dimensional heat equation rely on several simplifying assumptions. Consider a one-dimensional rod, which is assumed to be homogeneous and isotropic, with constant material parameters such as thermal conductivity k, density ρ, specific heat c, and a temperature field $u(x,t)$. The heat flux $q(x,t)$, defined as the heat flow per unit area, is taken to be positive in the $+x$ direction. Heat conduction is assumed to occur exclusively along the longitudinal direction, allowing for the neglect of transverse temperature gradients. Furthermore, internal heat generation is ignored, and radiative and convective heat losses are not included. The derivation is based on an Eulerian control volume approach, in which a slice of the rod fixed in space represents the control volume through which heat flows [16], where positive heat flux is defined as entering the control volume.

6.1.1 Energy Balance

The first law of thermodynamics (1) implies that any change in internal energy is equal to the difference between the heat entering and leaving the system, since no work is done.

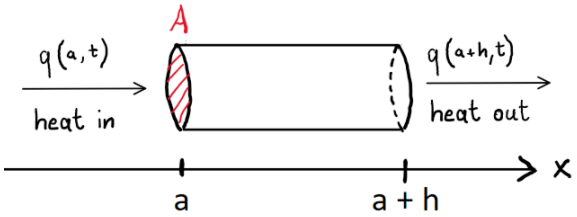

Figure 8: Visualisation of the Energy Balance: heat entering at $x = a$: $q(a,t)$, heat leaving at $x = a + h$: $q(a + h, t)$. [Author's Own]

The rate of change of internal energy can be expressed using its physical definition in terms of temperature. This leads to the following expression for the rate of change of internal energy within the slice $[a, a + h]$:

$$A\,[q(a,t) - q(a+h,t)] = \frac{d}{dt}\left(A\int_a^{a+h} \rho c\, u\, dx\right)$$

Here, multiplication by the cross-sectional area A converts the heat flux into the total heat flow through the control volume.

6.1.2 Constitutive relation for the heat flux

Using Fourier's law of heat conduction (2), the heat flux is expressed in terms of the temperature gradient. Dividing both sides of the energy balance by the cross-sectional area A then yields

$$-k\frac{\partial u}{\partial x}(a,t) + k\frac{\partial u}{\partial x}(a+h,t) = \frac{d}{dt}\left(\int_a^{a+h} \rho c\, u(x,t)\, dx\right).$$

Thus, the cross-sectional area cancels out, reflecting the one-dimensional nature of the problem.

6.1.3 Application of Leibniz' rule

As the integration limits are independent of time and the temperature function $u(x,t)$ is assumed to be sufficiently smooth, Leibniz' rule allows the time derivative to be taken inside the integral:

$$\frac{d}{dt}\left(\int_a^{a+h} \rho c\, u(x,t)\, dx\right) = \int_a^{a+h} \rho c\, \frac{\partial u}{\partial t}(x,t)\, dx.$$

6.1.4 Limit of an infinitesimal slice

Dividing both sides of the equation by the slice thickness h yields

$$\frac{k}{h}\left[\frac{\partial u}{\partial x}(a+h,t) - \frac{\partial u}{\partial x}(a,t)\right] = \frac{1}{h}\int_a^{a+h} \rho c\, \frac{\partial u}{\partial t}\, dx.$$

Taking the limit as $h \to 0$, the difference quotient of the temperature gradient converges to the second spatial derivative of the temperature, while the right-hand side approaches the local rate of change of internal energy per unit volume:

$$k\frac{\partial^2 u}{\partial x^2} = \rho c\frac{\partial u}{\partial t}.$$

6.1.5 Final form of the heat equation

Introducing the thermal diffusivity

$$\alpha = \frac{k}{\rho c},$$

the one-dimensional heat equation (7) is obtained:

$$\frac{\partial u}{\partial t} = \alpha\frac{\partial^2 u}{\partial x^2} \tag{11}$$

6.2 Analytical Solution Methods

6.2.1 Method 1: Separation of Variables for Fixed Boundary Conditions (Experiment 1)

In this section, the one-dimensional heat equation is solved analytically using the method of separation of variables, which is applicable under homogeneous [17] boundary conditions and suitable initial conditions. When the initial temperature distribution is constant, the resulting solution can be expressed in a particularly simple closed form. Experiment 1 is therefore chosen for comparison, as it satisfies all required conditions and, in addition, exhibits an approximately linear initial temperature profile. The general theory underlying this method, including the derivation of the separated ordinary differential equations (9), has already been presented in Section 4. Here, the focus lies on applying this method to the specific physical configuration of heating at one end.

Starting from the separation ansatz (8), the one-dimensional heat equation

$$\frac{\partial u}{\partial t} = \alpha \frac{\partial^2 u}{\partial x^2}$$

can be rewritten as

$$X(x)T'(t) = \alpha X''(x)T(t).$$

Dividing both sides by $\alpha X(x)T(t)$ yields

$$\frac{1}{\alpha}\frac{T'(t)}{T(t)} = \frac{X''(x)}{X(x)}.$$

Since the left-hand side depends only on time and the right-hand side only on space, both sides must be equal to a constant. Introducing the separation constant $-\lambda$ leads to the uncoupled ordinary differential equations

$$\begin{aligned} X''(x) + \lambda X(x) &= 0, \\ T'(t) + \lambda \alpha T(t) &= 0. \end{aligned} \tag{12}$$

The choice $\lambda > 0$ ensures oscillatory spatial solutions and excludes unbounded spatial solutions or temporal growth, which would be unphysical for a finite rod.

Temporal Solution The temporal equation

$$T'(t) + \lambda \alpha T(t) = 0$$

is a first-order linear ordinary differential equation. Its general solution is given by

$$T(t) = C\,\mathrm{e}^{-\lambda \alpha t} \tag{13}$$

where the exponential decay reflects the gradual equilibration of temperature differences over time. The value of λ cannot be determined from the temporal equation alone, as neither the initial condition nor the boundary conditions impose constraints on it.

Spatial Solution The spatial equation

$$X''(x) + \lambda X(x) = 0$$

is a second-order linear ordinary differential equation. For $\lambda > 0$, its general solution is

$$X(x) = A\cos\left(\sqrt{\lambda}x\right) + B\sin\left(\sqrt{\lambda}x\right) \tag{14}$$

In contrast to the temporal ODE, the admissible values of λ are fixed by the boundary conditions imposed on the system, for example, the mixed boundary conditions as used in the experimental setup. The admissible values of λ and the corresponding spatial solutions are therefore referred to as the *eigenvalues and eigenfunctions* of the associated spatial problem [2, p. 190]. More possible boundary conditions and their corresponding eigenvalues and eigenfunctions can be found in the Appendix B.

Mixed Boundary Conditions For a rod of length L with one end held at a constant temperature and the other thermally insulated,

$$u(0,t) = T_{\text{source}}, \qquad u_x(L,t) = 0,$$

where T_{source} denotes the fixed temperature imposed at the left boundary.

Since separation of variables requires homogeneous boundary conditions, the solution is written as a superposition of a steady-state solution and a transient component. The steady-state solution $u_s(x)$ satisfies

$$u_s''(x) = 0, \qquad u_s(0) = T_{\text{source}}, \qquad u_s'(L) = 0.$$

In the absence of internal heat sources, the steady-state temperature must be spatially uniform, yielding

$$u_s(x) = T_{\text{source}} \tag{15}$$

Defining the deviation from steady state

$$v(x,t) = u(x,t) - T_{\text{source}} \tag{16}$$

the transformed problem satisfies homogeneous boundary conditions

$$v(0,t) = 0, \qquad v_x(L,t) = 0,$$

and can therefore be solved using separation of variables. Hereafter, the analytical solution is constructed for $v(x,t)$.

The spatial boundary conditions imply

$$X(0) = 0 \quad \Rightarrow \quad A = 0,$$

and

$$X'(L) = 0 \quad \Rightarrow \quad \cos\Big(\sqrt{\lambda}L\Big) = 0.$$

Non-trivial solutions (not $X(x) = 0$) exist only if

$$\sqrt{\lambda}L = \frac{(2n+1)\pi}{2}, \qquad n = 0, 1, 2, \ldots$$

which leads to the discrete eigenvalues

$$\lambda_n = \left(\frac{(2n+1)\pi}{2L}\right)^2 \tag{17}$$

and corresponding eigenfunctions

$$X_n(x) = \sin\left(\frac{(2n+1)\pi x}{2L}\right) \tag{18}$$

Separated Solutions and Superposition For each eigenvalue λ_n, a separated solution of the transformed heat equation for $v(x,t)$ is obtained as

$$v_n(x,t) = B_n \, \mathrm{e}^{-\alpha\left(\frac{(2n+1)\pi}{2L}\right)^2 t} \sin\left(\frac{(2n+1)\pi x}{2L}\right).$$

where the constants B_n absorb the separation constants arising from the temporal solution.

By linear superposition, the general solution for the deviation from steady state is

$$v(x,t) = \sum_{n=0}^{\infty} B_n \, \mathrm{e}^{-\alpha\left(\frac{(2n+1)\pi}{2L}\right)^2 t} \sin\left(\frac{(2n+1)\pi x}{2L}\right) \tag{19}$$

Transforming back to the physical temperature yields

$$\boxed{u(x,t) = T_{\text{source}} + \sum_{n=0}^{\infty} B_n \, \mathrm{e}^{-\alpha\left(\frac{(2n+1)\pi}{2L}\right)^2 t} \sin\left(\frac{(2n+1)\pi x}{2L}\right)} \tag{20}$$

Determination of the Fourier Coefficients The initial temperature profile determines the coefficients B_n

$$u(x,0) = f(x).$$

In terms of the deviation variable $v(x,t)$, the initial condition becomes

$$v(x,0) = f(x) - T_{\text{source}}.$$

Setting $t = 0$ in the series solution gives

$$f(x) - T_{\text{source}} = \sum_{n=0}^{\infty} B_n \sin\left(\frac{(2n+1)\pi x}{2L}\right),$$

which represents a Fourier sine series adapted to the mixed boundary conditions [2, p. 219]. The coefficients are therefore [3, p. 56]

$$B_n = \frac{2}{L} \int_0^L (f(x) - T_{\text{source}}) \sin\left(\frac{(2n+1)\pi x}{2L}\right) dx \tag{21}$$

6.2.2 Comparison with Experiment 1

Having derived an analytical solution of the one-dimensional heat equation under the assumption of a constant function describing the initial condition, this section examines how well these solutions describe the experimentally observed temperature evolution in the first experiment. The goal is not to achieve perfect quantitative agreement, but rather to assess whether the heat equation captures the dominant physical behaviour and to identify systematic deviations arising from experimental limitations.

Insertion of Experimental Parameters The analytical solution obtained in Section 6.2.1 depends on four key inputs:

- the imposed boundary temperature T_{source},
- the length of the rod L,

- the thermal diffusivity α,
- the initial temperature distribution $f(x)$.

For Experiment 1, the left boundary of the rod was maintained at an approximately constant temperature of

$$T_{\text{source}} = 110^{\circ}\text{C},$$

which corresponds to a Dirichlet boundary condition at $x = 0$. The right end of the rod was thermally insulated, corresponding to a Neumann boundary condition at $x = L$, with

$$L = 0.3\,\text{m}.$$

The thermal diffusivity was estimated experimentally in Section 5.4.4 as

$$\alpha \approx 1.9 \times 10^{-4}\,\text{m}^2\,\text{s}^{-1}.$$

Although this value exceeds the tabulated diffusivity of aluminium, it is retained for the analytical model in order to ensure internal consistency between experiment and theory.

The initial temperature distribution was approximately uniform and close to ambient room temperature:

$$f(x) \approx 22^{\circ}\text{C}.$$

This implies that the transient component initially dominates the temperature evolution, while the steady-state contribution remains constant in space.

Substituting these experimental parameters into the analytical solution yields

$$u_{\text{theory}}(x,t) = 110 + \sum_{n=0}^{\infty} B_n \exp\left[-1.9 \times 10^{-4} \left(\frac{(2n+1)\pi}{2 \times 0.3}\right)^2 t\right] \sin\left(\frac{(2n+1)\pi x}{2 \times 0.3}\right), \tag{22}$$

where the initial temperature profile determines the coefficients B_n.

Evaluation of the Fourier Coefficients In the experiment, the initial temperature distribution was approximately uniform and equal to ambient room temperature,

$$f(x) \approx T_0 = 22^{\circ}\text{C}.$$

Thus,

$$f(x) - T_{\text{source}} = 22 - 110 = -88^{\circ}\text{C}.$$

Substituting this into the coefficient formula yields

$$B_n = \frac{2}{L} \int_0^L (-88) \sin\left(\frac{(2n+1)\pi x}{2L}\right) dx.$$

Evaluating the integral gives

$$\boxed{B_n = -\frac{352}{(2n+1)\pi}} \tag{23}$$

Since the initial temperature is constant in space, the Fourier coefficients can be evaluated analytically, resulting in a simple closed-form expression. As examples, the first three coefficients

are therefore

$$B_0 = -\frac{352}{\pi} \approx -112.0,$$
$$B_1 = -\frac{352}{3\pi} \approx -37.3,$$
$$B_2 = -\frac{352}{5\pi} \approx -22.4.$$

The negative sign reflects the fact that the rod is initially colder than the imposed boundary temperature and must warm up toward equilibrium.

Discrete Comparison Procedure Using Experimental Sampling To compare the analytical solution of the one-dimensional heat equation with the experimental data in a consistent manner, the theoretical temperature field is evaluated only at the discrete spatial locations and time instants at which measurements were taken. No spatial or temporal interpolation is applied.

The analytical solution derived in Section 6.2.1 is sampled at the same sensor positions and measurement times as the experimental data and plotted alongside the corresponding measurements. This allows a direct visual comparison of the temporal and spatial evolution of temperature along the rod.

Discrete Evaluation of the Analytical Solution At each sensor position x_i and measurement time t_j, the analytical temperature is given by

$$u_{\text{theory}}(x_i, t_j) = T_{\text{source}} + \sum_{n=0}^{N} B_n \exp\left[-\alpha \left(\frac{(2n+1)\pi}{2L}\right)^2 t_j\right] \sin\left(\frac{(2n+1)\pi x_i}{2L}\right), \tag{24}$$

where $N = 1000$ modes are retained. This relatively large truncation order is chosen to suppress visible Gibbs oscillations caused by the discontinuity between the initial temperature distribution and the imposed boundary condition [3, p. 59]. The additional higher-order modes decay rapidly in time and, therefore, do not influence the qualitative physical behaviour of the solution. The theoretical solution is evaluated slightly inside the domain rather than exactly at $x = 0$, since the boundary temperature is imposed ideally and is not directly comparable to surface-mounted sensor measurements. A full table in the same format as the experimental data can be found in the Appendix 5.

Qualitative Comparison The comparison involves setting the plots from the first experiment (Figures 4 and 5) side by side with the same type of plots depicting the analytical values. Emphasis is placed on the overall shape of the temperature profiles, the relative ordering of sensor readings, the temporal smoothing of temperature gradients, and the rate at which the system approaches thermal equilibrium.

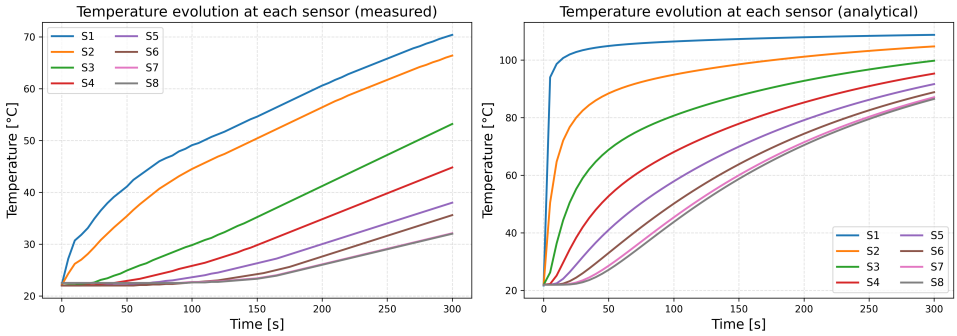

Figure 9: Temperature as a function of time for selected sensor positions in Experiment 1, measured (left) and predicted by the mathematical model (right). [Author's Own]

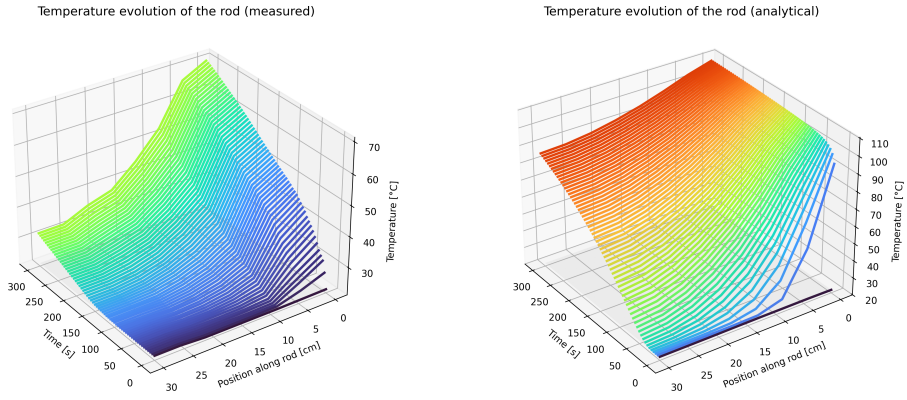

Figure 10: Spatio-temporal evolution of the temperature along the rod in Experiment 1, measured (left) and predicted by the mathematical model (right). [Author's Own]

Interpretation This discrete comparison procedure ensures that the analytical solution and the experimental data are compared under identical sampling conditions, avoiding distortions caused by interpolation or rescaling. The resulting plots therefore allow a direct qualitative assessment of the extent to which the heat equation reproduces the observed physical behaviour.

In particular, the comparison highlights:

- the qualitative propagation of heat along the rod,
- the progressive smoothing of temperature gradients over time,
- systematic discrepancies attributable to heat losses, sensor placement, and idealised boundary conditions.

The analytical solution thus provides a clear physical reference against which the experimental temperature evolution can be interpreted.

Discussion of Agreement and Deviations The analytical solution reproduces the qualitative behaviour observed in the experiment: Figure 9 shows that temperature changes propagate gradually along the rod and spatial gradients decrease over time, while Figure 10 features higher-frequency components decaying more rapidly than large-scale structures, consistent with the experimental observations. These observations are consistent with the mathematical structure of the heat equation and with the exponential decay of higher-order modes.

Quantitative discrepancies are observed, especially at later times and larger distances from the heat source. These deviations can be attributed to several factors neglected in the analytical model, including heat losses to the surrounding air, finite rod thickness, and the use of surface-mounted temperature sensors. Additionally, the assumption of perfectly constant boundary temperature is only approximately satisfied in the experiment.

Despite these limitations, the overall agreement supports the validity of modelling the experimental system using the one-dimensional heat equation. The analytical solution therefore serves as a clear physical reference against which the experimental temperature evolution can be interpreted.

6.2.3 Method 2: Fourier Transform Solution for Infinite Domain (Experiment 2)

The second experiment differs fundamentally from the first in that no external heat is supplied during the measurement period, and no fixed boundary temperatures are imposed. Instead, the temperature evolution is governed purely by the diffusion of an initially localised temperature distribution. This configuration is particularly well suited to an analytical treatment using the Fourier transform, which provides solutions of the heat equation on an infinite spatial domain.

In this approach, the rod is idealised as infinitely long, and boundary effects at the ends of the rod are neglected. This approximation is justified for early times, during which the thermal disturbance remains confined to the interior of the rod and has not yet interacted significantly with the boundaries. Since the initial temperature peak is located near the centre of the rod and the observed temperature profiles remain approximately symmetric, the infinite-domain assumption provides a physically meaningful description of the dominant heat diffusion process.

Definition of the Fourier Transform [3, p. 63] The Fourier transform provides a powerful alternative method for solving the heat equation, particularly suitable for problems on infinite or semi-infinite domains. The key idea is to transform the partial differential equation into an ordinary differential equation by eliminating the spatial derivative.

The Fourier transform of a function $u(x,t)$ with respect to the spatial variable x is defined as

$$\hat{u}(k,t) = \mathcal{F}\{u(x,t)\} = \int_{-\infty}^{\infty} u(x,t)e^{-ikx}\,dx, \tag{25}$$

where k is the frequency variable (wave number). The inverse Fourier transform allows recovery of the original function:

$$u(x,t) = \mathcal{F}^{-1}\{\hat{u}(k,t)\} = \frac{1}{2\pi}\int_{-\infty}^{\infty} \hat{u}(k,t)e^{ikx}\,dk. \tag{26}$$

The detailed properties of the Fourier transform are presented in Appendix C.

A crucial property of the Fourier transform is that differentiation in physical space corresponds to multiplication in frequency space [3, p. 63]. Specifically,

$$\mathcal{F}\left\{\frac{\partial^2 u}{\partial x^2}\right\} = -k^2\hat{u}(k,t). \tag{27}$$

Applying the Fourier transform to both sides of the heat equation

$$\frac{\partial u}{\partial t} = \alpha\frac{\partial^2 u}{\partial x^2}$$

yields

$$\frac{\partial \hat{u}}{\partial t} = -\alpha k^2 \hat{u}(k,t) \tag{28}$$

Since the Fourier transform is taken only with respect to x, the time derivative passes through unchanged. The resulting equation is a first-order ordinary differential equation in time for each frequency component k. This equation is structurally identical to equation (4) and has the solution

$$\hat{u}(k,t) = \hat{u}(k,0)e^{-\alpha k^2 t} \tag{29}$$

where $\hat{u}(k,0)$ is the Fourier transform of the initial condition $f(x) = u(x,0)$.

To obtain the temperature distribution in physical space, the inverse Fourier transform is applied:

$$u(x,t) = \frac{1}{2\pi} \int_{-\infty}^{\infty} \hat{u}(k,0)\, e^{-\alpha k^2 t}\, e^{ikx}\, dk. \tag{30}$$

Substituting the definition of $\hat{u}(k,0)$ as the Fourier transform of $f(x)$ gives

$$u(x,t) = \frac{1}{2\pi} \int_{-\infty}^{\infty} \left[\int_{-\infty}^{\infty} f(\xi) e^{-ik\xi}\, d\xi \right] e^{-\alpha k^2 t} e^{ikx}\, dk.$$

Rearranging the order of integration yields

$$u(x,t) = \int_{-\infty}^{\infty} f(\xi) \left[\frac{1}{2\pi} \int_{-\infty}^{\infty} e^{-\alpha k^2 t} e^{ik(x-\xi)}\, dk \right] d\xi.$$

The inner integral can be evaluated using the Gaussian integral formula [18]. Completing the square in the exponent:

$$-\alpha k^2 t + ik(x-\xi) = -\alpha t \left(k^2 - \frac{ik(x-\xi)}{\alpha t} \right) = -\alpha t \left(k - \frac{i(x-\xi)}{2\alpha t} \right)^2 - \frac{(x-\xi)^2}{4\alpha t}.$$

Substituting this result and using the standard Gaussian integral

$$\int_{-\infty}^{\infty} e^{-\alpha t\, k^2}\, dk = \sqrt{\frac{\pi}{\alpha t}},$$

the inner integral evaluates to

$$\frac{1}{2\pi} \int_{-\infty}^{\infty} e^{-\alpha k^2 t} e^{ik(x-\xi)}\, dk = \frac{1}{\sqrt{4\pi\alpha t}} \exp\left(-\frac{(x-\xi)^2}{4\alpha t} \right). \tag{31}$$

Therefore, the solution of the heat equation for an arbitrary initial condition $f(x)$ on an infinite domain is

$$\boxed{u(x,t) = \frac{1}{\sqrt{4\pi\alpha t}} \int_{-\infty}^{\infty} f(\xi) \exp\left(-\frac{(x-\xi)^2}{4\alpha t} \right) d\xi} \tag{32}$$

This is known as the *fundamental solution* or *Green's function* of the heat equation [19, p. 12]. The exponential kernel

$$G(x-\xi, t) = \frac{1}{\sqrt{4\pi\alpha t}} \exp\left(-\frac{(x-\xi)^2}{4\alpha t} \right) \tag{33}$$

represents the temperature distribution at time t resulting from an initial point source of heat at position ξ. The solution for any initial condition is obtained by superposition, integrating contributions from all points weighted by the initial temperature distribution.

Application to a Gaussian Initial Condition The measured initial temperature profile is smooth, symmetric, and strongly localised around the centre of the rod. It can therefore be well approximated by a Gaussian function of the form

$$f(x) = A \exp\left(-\frac{(x - x_0)^2}{2\sigma^2}\right), \tag{34}$$

where A represents the initial temperature amplitude, x_0 the position of the maximum, and σ characterises the spatial width of the heated region.

Substituting this initial condition into the fundamental solution yields

$$u(x,t) = \frac{1}{\sqrt{4\pi\alpha t}} \int_{-\infty}^{\infty} A \exp\left(-\frac{(\xi - x_0)^2}{2\sigma^2}\right) \exp\left(-\frac{(x-\xi)^2}{4\alpha t}\right) d\xi.$$

This integral can be evaluated by combining the two exponentials. Completing the square in ξ and using Gaussian integration yields the closed-form solution:

$$\boxed{u(x,t) = \frac{A\sigma}{\sqrt{\sigma^2 + 2\alpha t}} \exp\left(-\frac{(x - x_0)^2}{2(\sigma^2 + 2\alpha t)}\right)} \tag{35}$$

This result shows that a Gaussian initial condition remains Gaussian for all time under heat diffusion. The width of the distribution increases as $\sqrt{\sigma^2 + 2\alpha t}$, while the amplitude decreases proportionally to maintain conservation of total thermal energy. This property makes the Gaussian initial condition particularly tractable and provides a clear analytical prediction for comparison with Experiment 2.

6.2.4 Comparison to Experiment 2

Having derived an analytical solution of the one-dimensional heat equation under the assumption of a Gaussian function describing the initial condition, this section examines how well these solutions describe the experimentally observed temperature evolution in the second experiment. The goal is once again the same as before.

Insertion of Experimental Parameters To compare the analytical Fourier-transform solution with the experimental data from Experiment 2, the parameters A, x_0, and σ are determined from the initial measured temperature distribution. The thermal diffusivity α is taken from the value estimated in Section 5.4.4.

From the initial data at $t = 0$ (see Table 6):

- Peak temperature amplitude above ambient: $A \approx 11\,^\circ\mathrm{C}$ (peak of $33.5\,^\circ\mathrm{C}$ minus background)
- Peak position: $x_0 \approx 0.15\,\mathrm{m}$ (between sensors S4 and S5)
- Initial width: $\sigma \approx 0.04\,\mathrm{m}$ (estimated from the spatial extent of the initial profile)
- Thermal diffusivity: $\alpha = 1.9 \times 10^{-4}\,\mathrm{m^2\,s^{-1}}$

Substituting these values into the analytical solution yields:

$$u_{\text{theory}}(x,t) = T_{\text{ambient}} + \frac{11 \times 0.04}{\sqrt{0.04^2 + 2 \times 1.9 \times 10^{-4} \times t}} \exp\left(-\frac{(x - 0.15)^2}{2(0.04^2 + 2 \times 1.9 \times 10^{-4} \times t)}\right), \tag{36}$$

where $T_{\text{ambient}} \approx 22\,^\circ\mathrm{C}$ represents the background temperature.

Discrete Comparison Using Experimental Sampling Following the same procedure as in Section 6.2.2, the analytical solution is evaluated only at the discrete sensor positions and measurement times used in the experiment. No interpolation is applied, ensuring a direct comparison between theory and measurement.

Discrete Evaluation of the Analytical Solution At each sensor position x_i and measurement time t_j, the analytical temperature is given by

$$u_{\text{theory}}(x_i, t_j) = T_{\text{ambient}} + \frac{11 \times 0.04}{\sqrt{0.04^2 + 2 \times 1.9 \times 10^{-4} \times t}} \exp\left(-\frac{(x_i - 0.15)^2}{2(0.04^2 + 2 \times 1.9 \times 10^{-4} \times t_j)}\right), \tag{37}$$

where $T_{\text{ambient}} \approx 22°\text{C}$ represents the background temperature. The theoretical solution is again evaluated slightly inside the domain rather than exactly at $x = 0$, since the boundary temperature is imposed ideally and is not directly comparable to surface-mounted sensor measurements. A full table in the same format as the experimental data can be found in the Appendix 7.

Qualitative Comparison As before, the same types of plots are being compared.

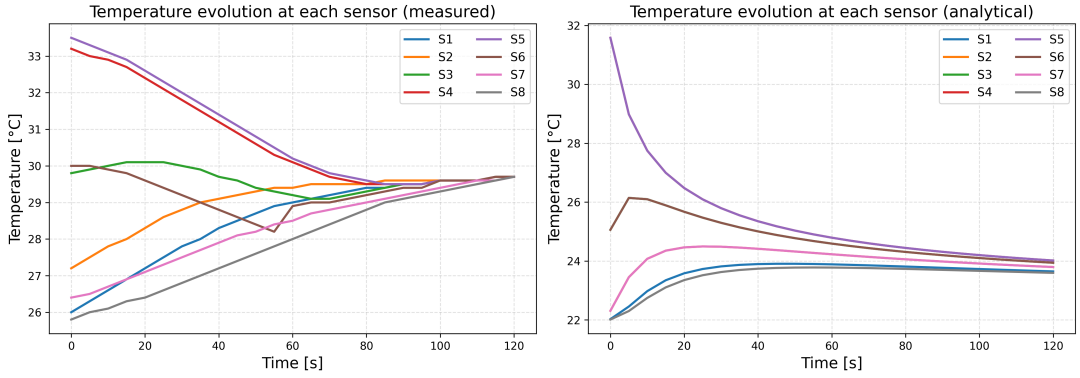

Figure 11: Temperature as a function of time for selected sensor positions in Experiment 2, measured (left) and predicted by the Fourier transform solution (right). [Author's Own]

Note that the right plot only shows the temperature of four positions, due to pairs of positions always having the same temperature, caused by the symmetrical structure of Gaussians (S1 and S8 deviate slightly since S1 was defined as $x = 0.01$).

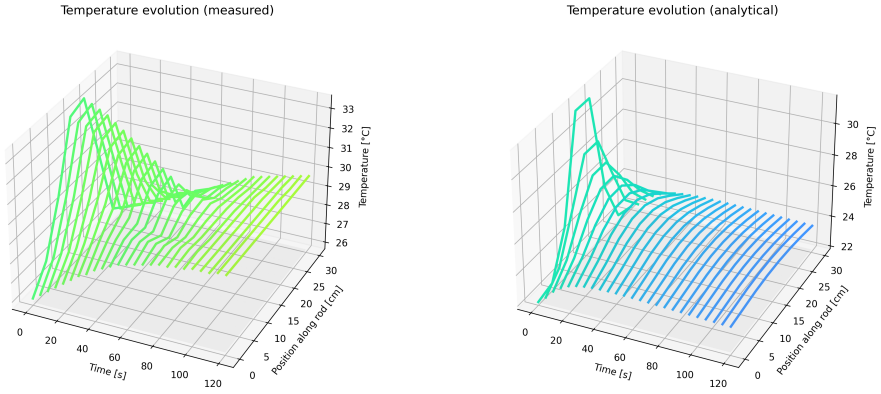

Figure 12: Spatio-temporal evolution of the temperature along the rod in Experiment 2, measured (left) and predicted by the Fourier transform solution (right). [Author's Own]

Interpretation The Fourier transform solution accurately reproduces the key qualitative features observed in Experiment 2:

- The symmetric, bell-shaped temperature profile centred near the middle of the rod
- The decay of the central temperature peak over time
- The initial increase followed by a decrease at sensors adjacent to the peak (S3, S6)
- The progressive flattening and widening of the temperature distribution

Discussion of Agreement and Deviations As shown in Figures 11 and 12, the analytical solution captures the dominant diffusion behaviour particularly well during the first 60-80 seconds of the experiment. During this interval, the thermal disturbance remains well within the rod boundaries, and the infinite-domain approximation is justified.

At later times, systematic deviations become apparent. The predicted temperatures converge towards a common value that lies below the measured temperature, indicating heat spreading outside the observed space, since the length of the rod is assumed to be infinite. This effect is partially captured by heat loss during the experiment, but the total heat energy inside the rod still lies well above what is predicted for this section. Additionally, as thermal energy approaches the rod boundaries, the infinite-domain assumption breaks down, and reflection effects at the insulated ends become relevant.

Despite these limitations, the agreement during the early diffusion phase validates the use of the one-dimensional heat equation and demonstrates the suitability of the Fourier transform approach for problems with localised initial conditions. The analytical solution provides clear physical insight into the Gaussian spreading behaviour characteristic of diffusive processes.

6.3 Conclusion: Analytical Solution Methods

The analytical investigation of the one-dimensional heat equation has demonstrated that the two complementary solution techniques- separation of variables with Fourier series and Fourier transform methods- provide powerful frameworks for understanding heat diffusion under different physical configurations. Both approaches have proven their value not only as mathematical tools but also as interpretive frameworks that reveal the underlying physics of thermal transport.

The comparison between analytical predictions and experimental observations establishes that the one-dimensional heat equation captures the dominant qualitative features of heat diffusion in the physical system studied. Both solution methods successfully reproduce the characteristic behaviours observed experimentally: the gradual propagation of thermal disturbances, the smoothing of spatial temperature gradients over time, and the progressive approach toward equilibrium states. The exponential decay of higher-order Fourier modes, explicitly present in both analytical solutions, directly corresponds to the observed rapid attenuation of fine-scale temperature variations. The Fourier series solution proves particularly well-suited for problems with fixed spatial boundaries and time-independent boundary conditions, as demonstrated in Experiment 1. The Fourier transform approach, applied to Experiment 2, excels in situations where initial conditions are localised and boundary effects are negligible during the timescale of interest. The analytical prediction of Gaussian spreading is confirmed by experimental observations during the early diffusion phase, illustrating the self-similar nature of diffusive processes.

Despite their predictive success, both analytical solutions introduce systematic deviations from experimental reality due to idealised assumptions. Heat losses to the surrounding environment

represent the most significant source of deviation, manifesting as temperature lag in Experiment 1 and average temperature decrease in Experiment 2. The finite thickness of the experimental rod and surface-mounted sensors introduce additional discrepancies, particularly during transient phases. In Experiment 2, the infinite-domain approximation breaks down at later times when thermal energy approaches the physical boundaries.

The complementarity of the two analytical approaches demonstrates their suitability for different classes of problems. Separation of variables naturally accommodates finite domains and reveals the modal structure of solutions, while the Fourier transform method provides direct insight into the dispersive character of heat diffusion through its frequency-domain perspective. Both methods embody the principle of linear superposition and expose the fundamental property that spatial patterns evolve through independent temporal decay of constituent modes. The qualitative agreement between analytical predictions and experimental observations, despite quantitative deviations arising from known physical effects, validates the one-dimensional heat equation as an appropriate mathematical model. The analytical solutions serve as reference solutions against which experimental reality can be interpreted and as essential benchmarks for the numerical methods presented in the following section.

6.4 Numerical Solution Methods

While analytical solutions provide valuable physical insight and serve as benchmarks for validation, they are limited to idealised geometries, simple boundary conditions, and specific initial distributions. Numerical methods extend the applicability of heat equation modelling to arbitrary configurations and allow complex scenarios to be investigated efficiently.

This section presents two complementary numerical approaches: the Forward Euler (Explicit) finite difference method for time-domain simulation, and the Fast Fourier Transform (FFT) method for spectral simulation in frequency space. Both methods will be implemented and visualised using Python and the Manim library in Section 7.

6.4.1 Forward Euler Method (Explicit Finite Difference)

The Forward Euler method, also known as the explicit finite difference method or Forward Time Centred Space (FTCS) scheme, is one of the simplest numerical approaches for solving parabolic partial differential equations such as the heat equation.

Discretisation The continuous spatial domain $[0, L]$ is divided into N equally spaced grid points with spacing

$$\Delta x = \frac{L}{N-1}, \tag{38}$$

and the time domain is discretised with uniform time step Δt. The temperature at position $x_i = i\Delta x$ and time $t_n = n\Delta t$ is denoted by $u_i^n \approx u(x_i, t_n)$.

Finite Difference Approximations The temporal derivative is approximated using a forward difference:

$$\left.\frac{\partial u}{\partial t}\right|_i^n \approx \frac{u_i^{n+1} - u_i^n}{\Delta t}, \tag{39}$$

and the spatial second derivative is approximated using a centred difference:

$$\left.\frac{\partial^2 u}{\partial x^2}\right|_i^n \approx \frac{u_{i+1}^n - 2u_i^n + u_{i-1}^n}{(\Delta x)^2}. \tag{40}$$

Explicit Update Scheme Substituting these approximations into the heat equation $u_t = \alpha u_{xx}$ yields

$$\frac{u_i^{n+1} - u_i^n}{\Delta t} = \alpha \frac{u_{i+1}^n - 2u_i^n + u_{i-1}^n}{(\Delta x)^2}. \tag{41}$$

Solving for the future value u_i^{n+1} gives the explicit update formula:

$$\boxed{u_i^{n+1} = u_i^n + r\left(u_{i+1}^n - 2u_i^n + u_{i-1}^n\right)} \tag{42}$$

where the dimensionless parameter

$$r = \frac{\alpha \Delta t}{(\Delta x)^2} \tag{43}$$

is known as the *mesh Fourier number* or *diffusion number* [20].

Stability Condition The Forward Euler method is only conditionally stable. For the scheme to remain stable and avoid unbounded oscillations, the diffusion number must satisfy the Courant–Friedrichs–Lewy (CFL) condition [21]:

$$\boxed{r = \frac{\alpha \Delta t}{(\Delta x)^2} \leq \frac{1}{2}} \tag{44}$$

This constraint limits the maximum allowable time step for a given spatial discretisation. Violating this condition results in numerical instability, with temperature values growing exponentially and producing unphysical results.

Advantages and Limitations The Forward Euler method is:

- **Simple to implement**: Only requires algebraic operations
- **Explicit**: Each grid point can be updated independently
- **Intuitive**: Directly reflects the physical diffusion process

However, it suffers from:

- **Conditional stability**: Requires small time steps for fine spatial grids
- **Low accuracy**: First-order accurate in time, second-order in space
- **Computational cost**: Small time steps increase the number of iterations needed

6.4.2 Fast Fourier Transform (FFT) Method

The Fast Fourier Transform (FFT) is a computationally efficient algorithm for computing the Discrete Fourier Transform (DFT). While the mathematical foundation of the Fourier transform is presented in Appendix C, this section addresses the numerical implementation.

Spectral Representation The Discrete Fourier Transform converts a sequence of N complex numbers $\{u_0, u_1, \ldots, u_{N-1}\}$ into another sequence $\{\hat{u}_0, \hat{u}_1, \ldots, \hat{u}_{N-1}\}$ according to [3, p. 66]:

$$\hat{u}_k = \sum_{n=0}^{N-1} u_n e^{-2\pi i k n/N}, \quad k = 0, 1, \ldots, N-1 \tag{45}$$

Direct evaluation of this sum requires $\mathcal{O}(N^2)$ operations[3, p. 68]—for each of the N output values $\hat{u}_k$, a sum over N input values must be computed.

The Fast Fourier Transform algorithm, developed by Cooley and Tukey in 1965 [22], reduces this computational complexity to $\mathcal{O}(N \log N)$ by exploiting the symmetry and periodicity properties of the complex exponential $e^{-2\pi i k n/N}$ [3, p. 65]. The key insight is to recursively decompose the DFT of size N into two DFTs of size N/2, continuing until reaching trivial base cases.

For N = 256 (as used in the simulations), the direct DFT would require approximately 65,536 complex multiplications, while the FFT requires only about 2,048—a factor of 32 speedup. This efficiency gain makes spectral methods practical for solving partial differential equations.

The inverse Fast Fourier Transform (IFFT) reconstructs the spatial representation from the frequency domain using [3, p. 66]:

$$u_n = \frac{1}{N} \sum_{k=0}^{N-1} \hat{u}_k e^{2\pi i k n/N}, \quad n = 0, 1, \ldots, N-1 \tag{46}$$

In Python, both transforms are implemented in the NumPy library:

```
u_hat = np.fft.fft(u)       # Forward FFT: spatial → frequency
u = np.fft.ifft(u_hat)      # Inverse FFT: frequency → spatial
```

The FFT algorithm requires N to be highly composite (ideally a power of 2 [3, p. 68]) for maximum efficiency. This is why $N = 256 = 2^8$ was chosen for the simulations rather than an arbitrary value.

For a detailed derivation of the Cooley-Tukey algorithm and its variants, see [3].

Numerical Implementation The FFT-based solution proceeds in three steps:

Step 1: Transform to frequency space

$$\hat{u}(k, 0) = \text{FFT}\{u(x, 0)\} \tag{47}$$

Step 2: Evolve each mode independently

$$\hat{u}(k, t) = \hat{u}(k, 0) \cdot e^{-\alpha k^2 t} \tag{48}$$

Step 3: Transform back to physical space

$$u(x, t) = \text{IFFT}\{\hat{u}(k, t)\} \tag{49}$$

Advantages and Limitations The FFT method offers:

- **Unconditional stability**: No CFL restriction on time step

- **High accuracy**: Spectral accuracy in space (exponential convergence for smooth solutions)
- **Computational efficiency**: Can take large time steps
- **Physical insight**: Directly reveals modal decay rates

However, it has limitations:

- **Boundary conditions**: Best suited for periodic boundaries; requires modifications for Dirichlet/Neumann conditions
- **Smoothness requirement**: Performance degrades for discontinuous solutions
- **Implementation complexity**: Requires careful handling of frequency indexing

Comparison of Methods Table 2 summarises the key differences between the two numerical methods:

Table 2: Comparison of numerical solution methods for the heat equation

Property	**Forward Euler**	**FFT Method**
Stability	Conditional ($r \leq 1/2$)	Unconditional
Spatial accuracy	$\mathcal{O}(\Delta x^2)$	Spectral
Temporal accuracy	$\mathcal{O}(\Delta t)$	Exact (for each mode)
Computational cost	$\mathcal{O}(N)$ per step	$\mathcal{O}(N \log N)$ per step
Time step size	Small (CFL limited)	Large (no restriction)
Boundary conditions	Flexible	Best for periodic
Implementation	Very simple	Moderate complexity

Both methods will be implemented in the simulation section and their performance compared for the experimental configurations studied in this work.

7 Simulation

While analytical solutions provide exact mathematical expressions and enable deep physical insight, visualisation plays a crucial role in developing intuition about the dynamic behaviour of heat diffusion. This section presents computer simulations of the heat equation using both the Forward Euler finite difference method and the Fast Fourier Transform spectral method described in Section 6.4. All visualisations and animations were created using Python with the Manim library [1], which allows for the generation of high-quality mathematical animations.

The simulations serve multiple purposes: they demonstrate the numerical implementation of both solution methods, illustrate the continuous time evolution of temperature distributions, and provide visual confirmation of the diffusion processes observed both analytically and experimentally. By comparing the two numerical approaches side by side, the relative advantages of explicit finite difference methods and spectral methods become apparent.

7.1 Implementation Overview

The simulation framework consists of several key components:

- **Forward Euler solver**: Python implementation of the explicit finite difference scheme discussed in Section 6.4.1
- **FFT solver**: Python implementation of the Fast Fourier Transform method discussed in Section 6.4.2 using the built-in `np.fft.fft()` and `np.fft.ifft()` NumPy library functions
- **Boundary condition handling**: Implementation of mixed (Experiment 1) and Neumann (Experiment 2) boundary conditions
- **Visualisation engine**: Manim-based rendering of temperature profiles and their continuous evolution
- **Parameter management**: Configuration of physical parameters (α, L), numerical parameters (Δx, Δt), and initial conditions

Three separate Manim programs were developed to simulate the different experimental configurations and numerical methods:

1. `HeatEquationMixedBCs_Euler.py`: Forward Euler method with mixed boundary conditions (Experiment 1)
2. `HeatEquationNeumann_Euler.py`: Forward Euler method with Neumann boundary conditions (Experiment 2)
3. `HeatEquation_FFT.py`: FFT spectral method with periodic/Neumann-like boundary conditions (Experiment 2)

The complete source code for all three programs, including detailed inline comments explaining each step, is provided in Appendix E.

7.2 Numerical Parameters and Stability

7.2.1 Forward Euler Method Parameters

The spatial domain is discretised into $N = 100$ grid points over a length $L = 0.3\,\text{m}$, giving a spatial step:

$$\Delta x = \frac{L}{N-1} = \frac{0.3}{99} \approx 0.00303\,\text{m} \tag{50}$$

To ensure numerical stability, the time step must satisfy the CFL condition derived in Appendix D:

$$r = \frac{\alpha \Delta t}{(\Delta x)^2} \leq \frac{1}{2} \tag{51}$$

For both Forward Euler simulations:

- Thermal diffusivity: $\alpha = 1.9 \times 10^{-4}\,\text{m}^2/\text{s}$
- Time step: $\Delta t = 0.005\,\text{s}$
- Resulting diffusion number: $r = \frac{1.9\times10^{-4}\times0.005}{(0.00303)^2} \approx 0.103 < 0.5$

Both simulations satisfy the stability criterion with a comfortable margin, ensuring that the numerical solution remains bounded and physically meaningful.

7.2.2 FFT Method Parameters

The FFT-based simulation uses different discretisation parameters optimised for spectral methods:

- Grid points: $N = 256 = 2^8$ (power of 2 for maximum FFT efficiency)
- Spatial step: $\Delta x = \frac{0.3}{255} \approx 0.00118\,\text{m}$
- Time step: $\Delta t = 1.0\,\text{s}$ (much larger than Forward Euler, no CFL restriction)
- Total simulation time: $t_{\max} = 120\,\text{s}$

The key advantage of the spectral method is that it is unconditionally stable, allowing much larger time steps than the Forward Euler method. This dramatically reduces the number of time iterations required (120 steps vs. 24,000 steps for Forward Euler over the same time period).

7.3 Simulation 1: Mixed Boundary Conditions (Forward Euler)

7.3.1 Problem Configuration

This simulation corresponds to the physical configuration of Experiment 1: one end of the rod is maintained at a fixed high temperature, while the other end is thermally insulated. The initial condition approximates the experimental measurements.

Boundary conditions:

$$u(0,t) = 110°\text{C} \quad \text{(left end: fixed temperature)} \tag{52}$$

$$\left.\frac{\partial u}{\partial x}\right|_{x=L} = 0 \quad \text{(right end: insulated)} \tag{53}$$

Initial condition: The initial temperature distribution is interpolated from the experimental data at $t = 0$.

Implementation details: The boundary values are enforced at every time step:

$$u_0^{n+1} = 110 \quad \text{(Dirichlet condition)} \tag{54}$$

$$u_{N-1}^{n+1} = u_{N-2}^{n+1} \quad \text{(Neumann condition, zero gradient approximation)} \tag{55}$$

7.3.2 Update Scheme

For interior points ($i = 1, 2, \ldots, N-2$), the Forward Euler update formula is applied:

$$u_i^{n+1} = u_i^n + \alpha \Delta t \frac{u_{i+1}^n - 2u_i^n + u_{i-1}^n}{(\Delta x)^2} \tag{56}$$

The simulation computes $n_{\text{steps}} = 60{,}000$ time steps over a total time of $t_{\max} = 300\,\text{s}$. To keep the animation manageable, only every 120th frame is stored and displayed, resulting in approximately 500 frames in the final animation.

7.3.3 Visualisation and Results

The Manim animation displays the continuous evolution of the temperature profile, compressed into an 8-second animation. Key features observed include:

- **Thermal front propagation**: Heat diffuses from the hot boundary (left) toward the insulated boundary (right)
- **Monotonic evolution**: Temperature at every interior point increases monotonically toward its steady-state value
- **Gradient smoothing**: Sharp initial gradients near the boundaries are progressively smoothed
- **Approach to steady state**: The profile gradually approaches a uniform steady

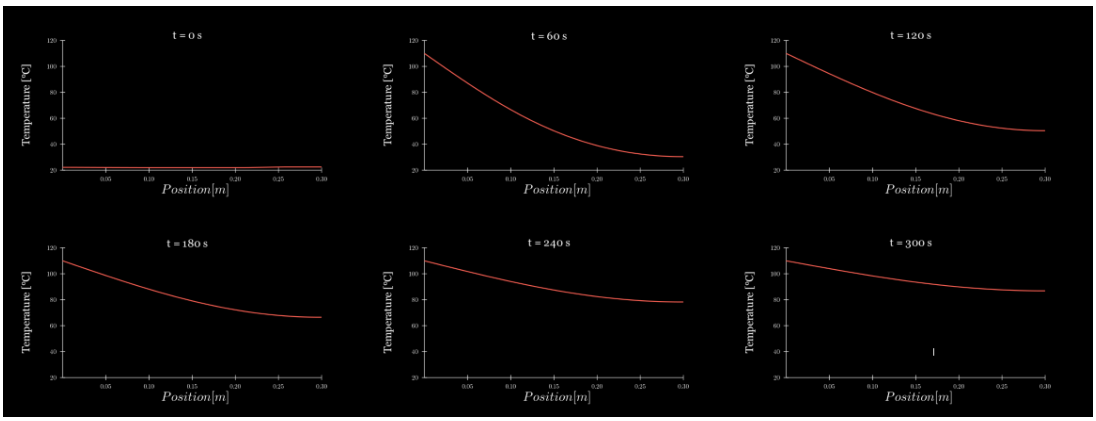

Figure 13: Selected snapshots from the mixed boundary condition simulation at times $t = 0, 60, 120, 180, 240, 300\,\text{s}$. The temperature profile evolves from the nearly uniform initial condition toward a steady state with continuous heating at the left boundary. [Author's Own]

The simulation qualitatively reproduces the behaviour observed in Experiment 1, where continuous heating at one end drives the system toward an equilibrium steady state.

7.4 Simulation 2a: Neumann Boundary Conditions (Forward Euler)

7.4.1 Problem Configuration

This simulation corresponds to an idealised version of Experiment 2: both ends of the rod are thermally insulated (zero heat flux), and the initial temperature distribution is a localised Gaussian peak representing the centred heating observed experimentally.

Boundary conditions (zero flux at both ends):

$$\left.\frac{\partial u}{\partial x}\right|_{x=0} = 0 \tag{57}$$

$$\left.\frac{\partial u}{\partial x}\right|_{x=L} = 0 \tag{58}$$

These are implemented numerically using symmetric boundary updates:

$$u_0^{n+1} = u_1^{n+1} \quad \text{(left boundary)} \tag{59}$$

$$u_{N-1}^{n+1} = u_{N-2}^{n+1} \quad \text{(right boundary)} \tag{60}$$

Initial condition (Gaussian temperature peak): The initial temperature distribution is interpolated from the experimental data at $t = 0$.

7.4.2 Update Scheme

The same Forward Euler formula is used for interior points. The Neumann boundary conditions ensure that no heat leaves the system, so the total thermal energy (integral of temperature) is conserved throughout the simulation.

The simulation computes $n_{\text{steps}} = 24{,}000$ time steps over $t_{\max} = 120\,\text{s}$, storing every 48th frame for animation.

7.4.3 Visualisation and Results

The animation shows the diffusion of the initially localised temperature peak. Observed phenomena include:

- **Symmetric spreading**: The Gaussian peak spreads symmetrically in both directions
- **Amplitude decay**: The peak temperature decreases as thermal energy distributes over a larger spatial extent
- **Width increase**: The spatial extent of the heated region grows proportional to $\sqrt{t}$, consistent with diffusive transport
- **Energy conservation**: The total thermal energy (area under the curve) remains constant within numerical precision

- **Approach to uniformity**: The system evolves toward a uniform temperature distribution equal to the spatial average of the initial profile

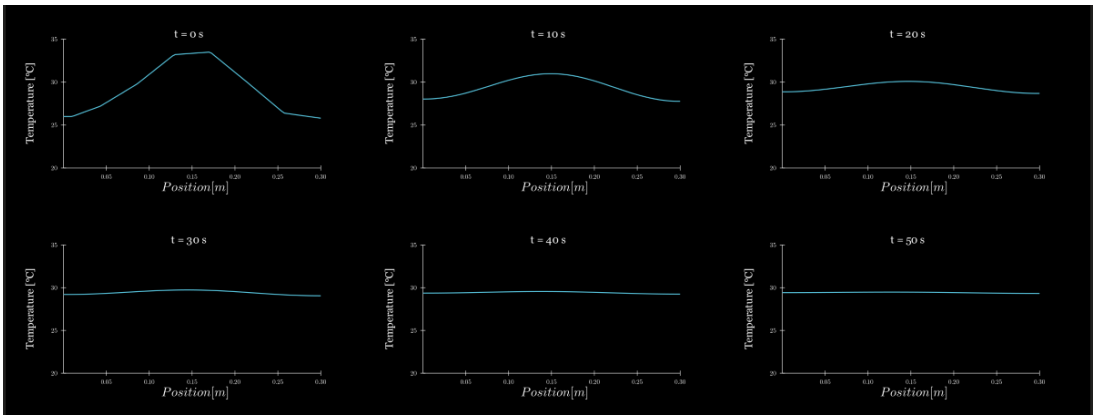

Figure 14: Selected snapshots from the Neumann boundary condition simulation (Forward Euler) at times $t = 0, 10, 20, 30, 40, 50\,\text{s}$. The initially sharp Gaussian peak progressively flattens and spreads while conserving total thermal energy. [Author's Own]

7.5 Simulation 2b: Neumann-like Conditions (FFT Spectral Method)

7.5.1 Problem Configuration

This simulation uses the same physical configuration as Simulation 2a but employs the FFT spectral method instead of Forward Euler. The FFT approach implicitly assumes periodic boundary conditions, but for a localised initial condition that remains well within the boundaries, the behaviour closely approximates Neumann conditions during the relevant time scales.

Initial condition Rather than using an idealised Gaussian, this simulation uses the actual interpolated experimental data from Experiment 2:

$$u(x, 0) = f(x) \quad \text{(interpolated from 8 sensor measurements)} \tag{61}$$

7.5.2 Spectral Update Scheme

The FFT method evolves the solution in three steps:

Step 1: Transform to frequency space

$$\hat{u}(k, 0) = \text{FFT}\{u(x, 0)\} \tag{62}$$

Step 2: Evolve each mode independently

$$\hat{u}(k, t) = \hat{u}(k, 0) \cdot e^{-\alpha k^2 t} \tag{63}$$

Each Fourier mode with wavenumber k decays exponentially at rate αk^2. Higher frequencies (representing finer spatial features) decay more rapidly, producing the characteristic smoothing effect of heat diffusion.

Step 3: Transform back to physical space

$$u(x, t) = \text{IFFT}\{\hat{u}(k, t)\} \tag{64}$$

The entire time evolution can be computed very efficiently: only 120 time steps are needed (compared to 24,000 for Forward Euler), each requiring only $\mathcal{O}(N \log N)$ operations for the FFT.

7.5.3 Visualisation and Results

The FFT simulation produces results that are visually indistinguishable from the Forward Euler simulation at the resolution shown, but with several key advantages:

- **Computational efficiency**: 200× fewer time steps required
- **Spectral accuracy**: Exponential convergence in space for smooth solutions
- **No stability restrictions**: Time step can be chosen based on accuracy requirements rather than stability
- **Physical insight**: Direct visualisation of how different spatial frequencies contribute to the solution

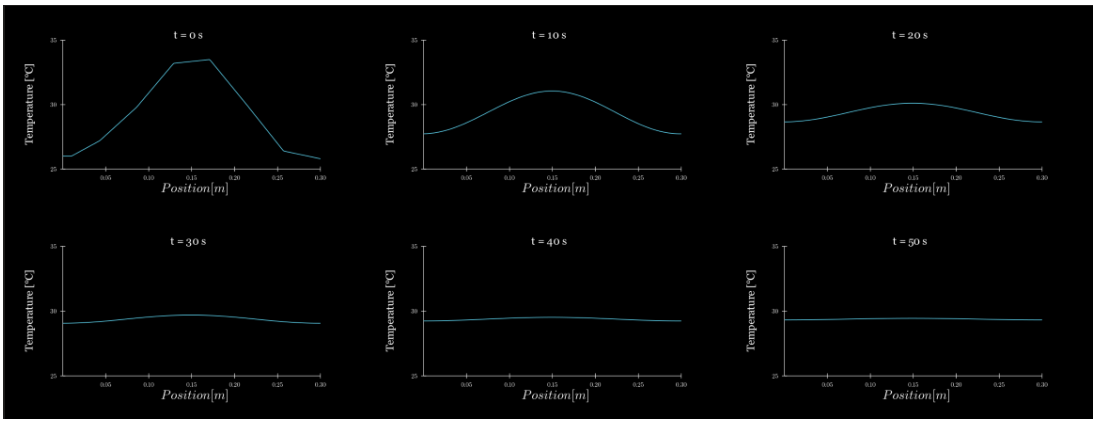

Figure 15: Selected snapshots from the FFT simulation at times $t = 0, 10, 20, 30, 40, 50\,\text{s}$. The temperature evolution is qualitatively identical to the Forward Euler simulation but computed much more efficiently. [Author's Own]

7.6 Comparison of Numerical Methods

Table 3 summarises the computational characteristics of the three simulations:

Table 3: Comparison of simulation parameters and computational requirements

Property	**Mixed BCs (Euler)**	**Neumann (Euler)**	**FFT (Spectral)**
Grid points N	100	100	256
Time step Δt (s)	0.005	0.005	1.0
Total time steps	60,000	24,000	120
Frames stored	500	500	120
Simulation time (s)	300	120	120
Diffusion number r	0.103	0.103	N/A
Stability condition	CFL: $r \leq 0.5$	CFL: $r \leq 0.5$	Unconditional
Spatial accuracy	$\mathcal{O}(\Delta x^2)$	$\mathcal{O}(\Delta x^2)$	Spectral
Temporal accuracy	$\mathcal{O}(\Delta t)$	$\mathcal{O}(\Delta t)$	Exact per mode

7.7 Conclusion: Numerical Solution Methods

The three simulations successfully demonstrate both the Forward Euler and FFT methods for solving the one-dimensional heat equation under different boundary conditions. Despite the Forward Euler simulations using relatively coarse spatial grids and small time steps to satisfy the CFL stability condition, they produce smooth, physically realistic temperature evolution that agrees qualitatively with both analytical predictions and experimental observations.

The FFT simulation highlights the power of spectral methods: by working in frequency space where each mode evolves independently, the method achieves high accuracy with dramatically fewer computational steps. The price paid for this efficiency is reduced flexibility in handling non-periodic boundary conditions and less intuitive implementation.

The animations provide valuable pedagogical insight by making abstract mathematical solutions tangible and visual. Observing the continuous evolution of temperature profiles reinforces understanding of key concepts such as:

- The directional flow of heat from regions of high to low temperature
- The smoothing effect of diffusion on sharp temperature gradients
- The distinction between transient and steady-state behaviour
- The role of boundary conditions in determining long-time system behaviour
- The conservation of thermal energy under insulated (Neumann) boundaries
- The independent evolution and decay of different spatial frequency components

The qualitative agreement between simulations, analytical solutions, and experimental observations validates the one-dimensional heat equation as an appropriate mathematical model for the physical systems studied in this work. Both numerical methods, despite their very different approaches, successfully capture the essential physics of heat diffusion.

8 Overall Conclusion

This investigation has demonstrated that the one-dimensional heat equation provides a robust mathematical framework for describing thermal diffusion in solid bodies, connecting theoretical predictions with observable physical behaviour through both analytical and numerical solution methods. The research objectives posed at the outset have been systematically addressed through a combination of experimental observation, mathematical analysis, and computational simulation.

Two complementary experimental configurations were successfully implemented to observe heat diffusion in a one-dimensional body: continuous heating at one end of an insulated metal rod, and diffusion from a localised temperature peak at the centre. Multiple temperature sensors enabled temporal and spatial resolution of the temperature field, providing data suitable for quantitative comparison with theoretical predictions. The experimental challenges encountered underscore the importance of careful system design when validating mathematical models.

The heat equation was solved using multiple approaches, each revealing different aspects of the underlying physics. Analytically, separation of variables with Fourier series proved effective for fixed boundary conditions, yielding modal solutions that decay exponentially in time, whilst Fourier transform methods provided closed-form solutions for localised initial conditions, revealing the Gaussian spreading characteristic of diffusive processes. Numerically, the Forward Euler method offered straightforward implementation with CFL stability constraints, whilst the FFT spectral method achieved 200-fold computational efficiency through frequency-space evolution. Each method exhibited distinct advantages in accuracy, stability, and implementation complexity.

Both analytical and numerical solutions captured the dominant qualitative features observed experimentally: gradual thermal propagation, spatial gradient smoothing, and exponential decay of higher-order modes. Quantitative agreement was best during early times and near heat sources, with systematic deviations appearing at later times due to heat losses, finite geometry effects, and imperfect boundary conditions. The thermal diffusivity estimated from experimental data exceeded tabulated values for aluminium, reflecting cumulative effects of idealisation. Despite these limitations, the overall correspondence validates the heat equation as an appropriate model for the physical system. The mathematical techniques employed extend far beyond thermal conduction, revealing their power across diverse areas of physics and mathematics. Separation of variables and Fourier methods appear in other partial differential equations such as the wave equation and Laplace's equation. In fluid dynamics, similar approaches describe viscous diffusion and concentration gradients. The heat equation itself models chemical diffusion, biological population spread, and option pricing in mathematical finance. Fourier transform methods underpin signal processing and data compression. The conceptual framework of modal decomposition, where complex phenomena are separated into independent evolving modes, represents a powerful paradigm throughout classical and quantum physics.

9 Outlook

This work establishes solid foundations for understanding one-dimensional heat diffusion, but numerous extensions would enrich both the physical realism and mathematical sophistication of the investigation. Extending the analysis to two and three spatial dimensions introduces geometric spreading effects and anisotropic conduction, with cylindrical or spherical coordinates exhibiting qualitatively different behaviour. Irregular geometries necessitate finite element methods, whilst thermal imaging cameras could provide full spatial temperature fields for experimental validation, offering far richer datasets than discrete sensor measurements.

More complex boundary conditions present further opportunities for investigation.
Time-dependent boundary conditions, such as periodic heating or transient thermal shocks, generate forced responses that combine transient and driven components. Interface conditions between materials with different thermal properties introduce discontinuities that preclude analytical solutions and demonstrate the necessity of numerical methods. Robin boundary conditions, incorporating heat exchange with the environment, would enable a quantitative treatment of convective losses, addressing one of the primary sources of discrepancy between idealised models and experimental observations.

Relaxing the assumption of homogeneous material properties opens additional avenues for exploration. Spatially varying thermal conductivity, density, or specific heat capacity leads to modified partial differential equations where standard separation of variables fails. Temperature-dependent material properties introduce nonlinearity, requiring iterative numerical solution techniques. These extensions connect the idealised framework developed here to realistic engineering applications where material inhomogeneity and property variation play essential roles.

Whilst this investigation has thoroughly addressed its objectives within the one-dimensional framework, it simultaneously reveals a rich landscape of extensions awaiting exploration. The mathematical methods and physical insights developed here provide essential foundations for these more ambitious investigations, demonstrating that even seemingly simple systems contain layers of complexity that reward careful study.

A Experimental Data

This appendix provides the complete dataset measured in the experiments, together with discrete analytical data in the same format for comparison.

A.1 Complete Dataset of Experiment 1

Table 4: Complete temperature dataset measured in degrees Celsius for the aluminium rod.

t (s)	S1	S2	S3	S4	S5	S6	S7	S8
0	22.2	22.1	22.0	22.0	22.0	22.0	22.5	22.5
5	27.2	24.3	22.1	22.0	22.0	22.0	22.5	22.5
10	30.7	26.2	22.1	22.0	22.0	22.0	22.5	22.5
15	31.8	27.0	22.2	22.0	22.0	22.0	22.5	22.5
20	33.1	28.1	22.4	22.1	22.0	22.0	22.5	22.5
25	34.9	29.4	22.6	22.1	22.0	22.0	22.5	22.5
30	36.5	30.8	23.1	22.2	22.0	22.0	22.5	22.5
35	37.9	32.0	23.4	22.3	22.1	22.0	22.5	22.5
40	39.1	33.2	23.9	22.5	22.1	22.0	22.5	22.5
45	40.1	34.3	24.3	22.7	22.1	22.0	22.5	22.5
50	41.1	35.4	24.9	22.9	22.1	22.0	22.5	22.5
55	42.4	36.6	25.4	23.1	22.2	22.0	22.5	22.5
60	43.3	37.7	25.9	23.3	22.3	22.1	22.5	22.5
65	44.2	38.7	26.3	23.6	22.4	22.1	22.5	22.5
70	45.1	39.7	26.9	23.9	22.6	22.2	22.5	22.5
75	46.0	40.7	27.4	24.2	22.7	22.2	22.5	22.5
80	46.6	41.5	27.9	24.5	22.9	22.3	22.5	22.5
85	47.1	42.3	28.4	24.8	23.0	22.3	22.5	22.5
90	47.9	43.1	28.9	25.2	23.2	22.4	22.5	22.5
95	48.4	43.8	29.4	25.5	23.4	22.5	22.6	22.5
100	49.1	44.5	29.8	25.8	23.6	22.6	22.7	22.6
105	49.5	45.1	30.3	26.1	23.8	22.7	22.7	22.6
110	50.1	45.7	30.8	26.4	24.0	22.8	22.7	22.6
115	50.7	46.3	31.2	26.8	24.3	22.9	22.8	22.7
120	51.2	46.9	31.8	27.2	24.5	23.0	22.8	22.7
125	51.7	47.4	32.3	27.6	24.8	23.2	22.9	22.8
130	52.3	48.0	32.9	28.0	25.1	23.4	23.0	22.9
135	52.9	48.6	33.5	28.4	25.4	23.6	23.1	23.0
140	53.5	49.2	34.0	28.9	25.7	23.8	23.2	23.1
145	54.1	49.8	34.6	29.3	26.0	24.0	23.3	23.2
150	54.6	50.4	35.2	29.8	26.3	24.2	23.4	23.3
155	55.2	51.0	35.8	30.3	26.6	24.4	23.6	23.5
160	55.8	51.6	36.4	30.8	26.9	24.7	23.8	23.7
165	56.4	52.2	37.0	31.3	27.2	25.0	24.0	23.9
170	57.0	52.8	37.6	31.8	27.6	25.3	24.3	24.2
175	57.6	53.4	38.2	32.3	28.0	25.6	24.6	24.5
180	58.2	54.0	38.8	32.8	28.4	26.0	24.9	24.8
185	58.8	54.6	39.4	33.3	28.8	26.4	25.2	25.1
190	59.4	55.2	40.0	33.8	29.2	26.8	25.5	25.4

Continued on next page

t (s)	S1	S2	S3	S4	S5	S6	S7	S8
195	60.0	55.8	40.6	34.3	29.6	27.2	25.8	25.7
200	60.6	56.4	41.2	34.8	30.0	27.6	26.1	26.0
205	61.1	57.0	41.8	35.3	30.4	28.0	26.4	26.3
210	61.7	57.6	42.4	35.8	30.8	28.4	26.7	26.6
215	62.2	58.1	43.0	36.3	31.2	28.8	27.0	26.9
220	62.8	58.7	43.6	36.8	31.6	29.2	27.3	27.2
225	63.3	59.2	44.2	37.3	32.0	29.6	27.6	27.5
230	63.8	59.7	44.8	37.8	32.4	30.0	27.9	27.8
235	64.3	60.2	45.4	38.3	32.8	30.4	28.2	28.1
240	64.8	60.7	46.0	38.8	33.2	30.8	28.5	28.4
245	65.3	61.2	46.6	39.3	33.6	31.2	28.8	28.7
250	65.8	61.7	47.2	39.8	34.0	31.6	29.1	29.0
255	66.3	62.2	47.8	40.3	34.4	32.0	29.4	29.3
260	66.8	62.7	48.4	40.8	34.8	32.4	29.7	29.6
265	67.3	63.2	49.0	41.3	35.2	32.8	30.0	29.9
270	67.8	63.7	49.6	41.8	35.6	33.2	30.3	30.2
275	68.2	64.2	50.2	42.3	36.0	33.6	30.6	30.5
280	68.7	64.6	50.8	42.8	36.4	34.0	30.9	30.8
285	69.1	65.1	51.4	43.3	36.8	34.4	31.2	31.1
290	69.6	65.5	52.0	43.8	37.2	34.8	31.5	31.4
295	70.0	66.0	52.6	44.3	37.6	35.2	31.8	31.7
300	70.4	66.4	53.2	44.8	38.0	35.6	32.1	32.0

A.2 Analytical Solution Data for Experiment 1 (N=1000 modes)

Table 5: Analytical temperature values in degrees Celsius computed using separation of variables with 1000 Fourier modes for mixed boundary conditions.

t (s)	S1	S2	S3	S4	S5	S6	S7	S8
0	21.7	21.9	22.0	22.0	22.0	22.0	22.0	22.0
5	94.0	50.5	26.3	22.3	22.0	22.0	22.0	22.0
10	98.7	64.7	36.3	25.2	22.5	22.0	22.0	22.0
15	100.7	72.1	44.4	29.7	24.1	22.4	22.1	22.0
20	102.0	76.7	50.5	34.2	26.4	23.2	22.3	22.1
25	102.8	80.0	55.2	38.3	29.0	24.5	22.8	22.4
30	103.4	82.5	59.0	42.0	31.6	26.0	23.5	22.9
35	103.9	84.4	62.1	45.2	34.2	27.7	24.5	23.6
40	104.3	86.0	64.7	48.0	36.6	29.4	25.7	24.6
45	104.6	87.3	67.0	50.5	38.9	31.2	27.1	25.8
50	104.9	88.5	68.9	52.8	41.1	33.1	28.6	27.2
55	105.1	89.4	70.6	54.9	43.1	34.9	30.2	28.7
60	105.4	90.3	72.1	56.7	45.0	36.7	31.8	30.3
65	105.5	91.1	73.5	58.5	46.9	38.5	33.5	31.9
70	105.7	91.7	74.8	60.1	48.7	40.3	35.2	33.6
75	105.9	92.4	75.9	61.6	50.3	42.0	37.0	35.3
80	106.0	93.0	77.0	63.0	52.0	43.7	38.7	37.0
85	106.1	93.5	78.0	64.4	53.5	45.4	40.4	38.7

Continued on next page

t (s)	S1	S2	S3	S4	S5	S6	S7	S8
90	106.2	94.0	78.9	65.7	55.0	46.9	42.1	40.4
95	106.4	94.5	79.8	66.9	56.5	48.6	43.8	42.1
100	106.5	94.9	80.7	68.1	57.9	50.2	45.4	43.8
105	106.6	95.4	81.5	69.2	59.3	51.7	47.0	45.4
110	106.7	95.8	82.3	70.3	60.6	53.2	48.6	47.0
115	106.8	96.2	83.0	71.4	61.9	54.6	50.1	48.6
120	106.9	96.5	83.8	72.4	63.1	56.0	51.6	50.2
125	107.0	96.9	84.5	73.3	64.4	57.4	53.1	51.7
130	107.1	97.2	85.1	74.3	65.5	58.8	54.6	53.2
135	107.2	97.6	85.8	75.2	66.7	60.1	56.0	54.6
140	107.3	97.9	86.4	76.2	67.8	61.4	57.4	56.0
145	107.4	98.2	87.0	77.0	69.0	62.6	58.7	57.4
150	107.5	98.5	87.6	77.9	70.0	63.8	60.0	58.7
155	107.6	98.8	88.2	78.7	71.0	65.0	61.3	60.0
160	107.6	99.1	88.8	79.6	72.0	66.2	62.6	61.3
165	107.7	99.4	89.3	80.3	73.0	67.3	63.8	62.6
170	107.8	99.7	89.9	81.1	73.9	68.4	65.0	63.8
175	107.9	99.9	90.4	81.8	74.9	69.5	66.1	65.0
180	108.0	100.2	90.9	82.6	75.8	70.5	67.2	66.1
185	108.0	100.5	91.4	83.3	76.6	71.5	68.3	67.2
190	108.1	100.7	91.9	84.0	77.5	72.5	69.4	68.3
195	108.2	101.0	92.3	84.6	78.3	73.5	70.5	69.4
200	108.3	101.2	92.8	85.3	79.1	74.4	71.5	70.5
205	108.3	101.4	93.3	85.9	79.9	75.3	72.5	71.5
210	108.4	101.6	93.7	86.5	80.7	76.2	73.4	72.5
215	108.5	101.8	94.1	87.1	81.5	77.1	74.4	73.4
220	108.5	102.1	94.5	87.7	82.2	77.9	75.3	74.4
225	108.6	102.3	94.9	88.3	82.9	78.7	76.2	75.3
230	108.6	102.5	95.3	88.9	83.6	79.6	77.1	76.2
235	108.7	102.6	95.7	89.4	84.3	80.3	77.9	77.1
240	108.7	102.8	96.0	89.9	84.9	81.1	78.7	77.9
245	108.8	103.0	96.4	90.4	85.6	81.9	79.5	78.7
250	108.8	103.2	96.7	90.9	86.2	82.6	80.3	79.5
255	108.9	103.3	97.1	91.4	86.8	83.3	81.1	80.3
260	108.9	103.5	97.4	91.9	87.4	84.0	81.8	81.1
265	109.0	103.7	97.7	92.4	88.0	84.6	82.5	81.8
270	109.0	103.8	98.0	92.8	88.6	85.3	83.2	82.5
275	109.1	104.0	98.3	93.3	89.1	85.9	83.9	83.2
280	109.1	104.1	98.6	93.7	89.6	86.5	84.6	83.9
285	109.1	104.3	98.9	94.1	90.2	87.1	85.2	84.6
290	109.2	104.4	99.1	94.5	90.7	87.7	85.9	85.2
295	109.2	104.5	99.4	94.9	91.2	88.3	86.5	85.9
300	109.3	104.7	99.7	95.3	91.7	88.9	87.1	86.5

A.3 Complete Dataset of Experiment 2

Table 6: Complete temperature dataset measured in degrees Celsius for the aluminium rod heated in the middle.

t [s]	S1	S2	S3	S4	S5	S6	S7	S8
0	26.0	27.2	29.8	33.2	33.5	30.0	26.4	25.8
5	26.3	27.5	29.9	33.0	33.3	30.0	26.5	26.0
10	26.6	27.8	30.0	32.9	33.1	29.9	26.7	26.1
15	26.9	28.0	30.1	32.7	32.9	29.8	26.9	26.3
20	27.2	28.3	30.1	32.4	32.6	29.6	27.1	26.4
25	27.5	28.6	30.1	32.1	32.3	29.4	27.3	26.6
30	27.8	28.8	30.0	31.8	32.0	29.2	27.5	26.8
35	28.0	29.0	29.9	31.5	31.7	29.0	27.7	27.0
40	28.3	29.1	29.7	31.2	31.4	28.8	27.9	27.2
45	28.5	29.2	29.6	30.9	31.1	28.6	28.1	27.4
50	28.7	29.3	29.4	30.6	30.8	28.4	28.2	27.6
55	28.9	29.4	29.3	30.3	30.5	28.2	28.4	27.8
60	29.0	29.4	29.2	30.1	30.2	28.9	28.5	28.0
65	29.1	29.5	29.1	29.9	30.0	29.0	28.7	28.2
70	29.2	29.5	29.1	29.7	29.8	29.0	28.8	28.4
75	29.3	29.5	29.2	29.6	29.7	29.1	28.9	28.6
80	29.4	29.5	29.3	29.5	29.6	29.2	29.0	28.8
85	29.4	29.6	29.4	29.5	29.5	29.3	29.1	29.0
90	29.5	29.6	29.5	29.5	29.5	29.4	29.2	29.1
95	29.5	29.6	29.5	29.5	29.5	29.4	29.3	29.2
100	29.6	29.6	29.6	29.6	29.6	29.6	29.4	29.3
105	29.6	29.6	29.6	29.6	29.6	29.6	29.5	29.4
110	29.6	29.6	29.6	29.6	29.6	29.6	29.6	29.5
115	29.7	29.7	29.7	29.7	29.7	29.7	29.6	29.6
120	29.7	29.7	29.7	29.7	29.7	29.7	29.7	29.7

A.4 Analytical Solution Data for Experiment 2

Table 7: Analytical temperature values (in degrees Celsius) computed using Fourier transform method for Experiment 2 configuration.

t (s)	S1	S2	S3	S4	S5	S6	S7	S8
0	22.0	25.0	28.9	31.5	31.5	28.9	25.0	22.0
5	22.0	24.9	28.7	31.3	31.3	28.7	24.9	22.0
10	22.1	24.9	28.6	31.1	31.1	28.6	24.9	22.1
15	22.1	24.9	28.5	30.9	30.9	28.5	24.9	22.1
20	22.2	24.9	28.3	30.7	30.7	28.3	24.9	22.2
25	22.3	24.9	28.2	30.5	30.5	28.2	24.9	22.3
30	22.4	24.9	28.0	30.3	30.3	28.0	24.9	22.4
35	22.5	24.9	27.9	30.1	30.1	27.9	24.9	22.5
40	22.6	24.9	27.7	29.9	29.9	27.7	24.9	22.6
45	22.7	24.9	27.6	29.7	29.7	27.6	24.9	22.7

Continued on next page

t (s)	S1	S2	S3	S4	S5	S6	S7	S8
50	22.8	24.9	27.4	29.5	29.5	27.4	24.9	22.8
55	22.9	25.0	27.3	29.3	29.3	27.3	25.0	22.9
60	23.0	25.0	27.1	29.1	29.1	27.1	25.0	23.0
65	23.1	25.0	27.0	28.9	28.9	27.0	25.0	23.1
70	23.2	25.0	26.8	28.7	28.7	26.8	25.0	23.2
75	23.3	25.0	26.7	28.6	28.6	26.7	25.0	23.3
80	23.4	25.0	26.5	28.4	28.4	26.5	25.0	23.4
85	23.5	25.0	26.4	28.2	28.2	26.4	25.0	23.5
90	23.6	25.1	26.2	28.1	28.1	26.2	25.1	23.6
95	23.7	25.1	26.1	27.9	27.9	26.1	25.1	23.7
100	23.8	25.1	26.0	27.7	27.7	26.0	25.1	23.8
105	23.9	25.1	25.8	27.6	27.6	25.8	25.1	23.9
110	24.0	25.1	25.7	27.4	27.4	25.7	25.1	24.0
115	24.1	25.1	25.6	27.3	27.3	25.6	25.1	24.1
120	24.2	25.1	25.4	27.1	27.1	25.4	25.1	24.2

B Spatial Solution of the Heat Equation for different Boundary Conditions

This appendix derives the eigenvalues and eigenfunctions for other boundary conditions than those discussed in the main section and provides the key points of the derivation of the Fourier series. For the complete derivation, see [3].

B.1 Eigenvalue Problems for the One-Dimensional Laplacian

Consider the spatial ordinary differential equation

$$X''(x) + \lambda X(x) = 0$$

defined on the interval $[0, L]$.

For $\lambda > 0$, the general solution is

$$X(x) = A\cos\Big(\sqrt{\lambda}x\Big) + B\sin\Big(\sqrt{\lambda}x\Big).$$

B.1.1 Derivation of the General Solution

To determine the general solution of the spatial ordinary differential equation

$$X''(x) + \lambda X(x) = 0,$$

an exponential trial solution of the form

$$X(x) = \mathrm{e}^{rx} \tag{65}$$

is assumed.

Substituting this ansatz into the differential equation yields

$$r^2\mathrm{e}^{rx} + \lambda\mathrm{e}^{rx} = 0.$$

Since $e^{rx} \neq 0$, this leads to the characteristic equation

$$r^2 + \lambda = 0.$$

For $\lambda > 0$, the roots are

$$r = \pm i\sqrt{\lambda}.$$

The general solution can therefore be written as

$$X(x) = C_1 e^{i\sqrt{\lambda}x} + C_2 e^{-i\sqrt{\lambda}x}.$$

Using Euler's formula, this expression can be rewritten in real form as

$$X(x) = A\cos\Big(\sqrt{\lambda}x\Big) + B\sin\Big(\sqrt{\lambda}x\Big), \tag{66}$$

where $A, B \in \mathbb{R}$.

B.1.2 Dirichlet Boundary Conditions

The Dirichlet boundary conditions are

$$X(0) = 0, \qquad X(L) = 0.$$

Applying $X(0) = 0$ yields $A = 0$. Applying $X(L) = 0$ gives

$$\sin\Big(\sqrt{\lambda}L\Big) = 0.$$

Thus,

$$\sqrt{\lambda}L = n\pi, \qquad n = 1, 2, 3, \ldots$$

The eigenvalues and eigenfunctions are

$$\lambda_n = \left(\frac{n\pi}{L}\right)^2, \qquad X_n(x) = \sin\left(\frac{n\pi x}{L}\right). \tag{67}$$

The general solution of the corresponding heat equation is

$$u(x,t) = \sum_{n=1}^{\infty} B_n\, e^{-\alpha\left(\frac{n\pi}{L}\right)^2 t} \sin\left(\frac{n\pi x}{L}\right). \tag{68}$$

B.1.3 Neumann Boundary Conditions

The Neumann boundary conditions are

$$X'(0) = 0, \qquad X'(L) = 0.$$

Applying $X'(0) = 0$ yields $B = 0$. Applying $X'(L) = 0$ gives

$$\sin\Big(\sqrt{\lambda}L\Big) = 0.$$

Thus,

$$\sqrt{\lambda}L = n\pi, \qquad n = 0, 1, 2, \ldots$$

The eigenvalues and eigenfunctions are

$$\lambda_n = \left(\frac{n\pi}{L}\right)^2, \qquad X_n(x) = \cos\left(\frac{n\pi x}{L}\right). \tag{69}$$

For $n = 0$, the eigenfunction reduces to a constant, corresponding to the steady-state solution. The general solution of the corresponding heat equation is

$$u(x,t) = A_0 + \sum_{n=1}^{\infty} A_n \, \mathrm{e}^{-\alpha\left(\frac{n\pi}{L}\right)^2 t} \cos\left(\frac{n\pi x}{L}\right). \tag{70}$$

B.2 Fourier Series and Orthogonality

B.2.1 Orthogonality Relations

For integers $m, n \geq 1$, the following orthogonality relations hold on $[0, L]$:

$$\int_0^L \sin\left(\frac{n\pi x}{L}\right) \sin\left(\frac{m\pi x}{L}\right) \, dx = \begin{cases} 0, & n \neq m, \\ \frac{L}{2}, & n = m, \end{cases} \tag{71}$$

$$\int_0^L \cos\left(\frac{n\pi x}{L}\right) \cos\left(\frac{m\pi x}{L}\right) \, dx = \begin{cases} 0, & n \neq m, \\ \frac{L}{2}, & n = m, \end{cases} \tag{72}$$

$$\int_0^L \sin\left(\frac{n\pi x}{L}\right) \cos\left(\frac{m\pi x}{L}\right) \, dx = 0. \tag{73}$$

B.2.2 Fourier Series Representation

Let $f(x)$ be a piecewise continuous function on $[0, L]$. Its Fourier series expansion is given by

$$f(x) = \frac{A_0}{2} + \sum_{n=1}^{\infty} \left[A_n \cos\left(\frac{n\pi x}{L}\right) + B_n \sin\left(\frac{n\pi x}{L}\right) \right]. \tag{74}$$

B.2.3 Derivation of Fourier Coefficients

Multiplying the Fourier series by $\cos\left(\frac{m\pi x}{L}\right)$ and integrating over $[0, L]$ yields

$$A_m = \frac{2}{L} \int_0^L f(x) \cos\left(\frac{m\pi x}{L}\right) \, dx. \tag{75}$$

Similarly, multiplying by $\sin\left(\frac{m\pi x}{L}\right)$ gives

$$B_m = \frac{2}{L} \int_0^L f(x) \sin\left(\frac{m\pi x}{L}\right) \, dx. \tag{76}$$

The constant coefficient is given by

$$A_0 = \frac{2}{L} \int_0^L f(x) \, dx. \tag{77}$$

C Fourier Transform: Derivation and Properties

This appendix presents the mathematical foundation of the Fourier transform and its key properties that are used in Section 6.2.3 to solve the heat equation on an infinite domain. For the complete derivation with all the details, see [3].

C.1 Motivation: From Fourier Series to Fourier Transform

The Fourier transform can be understood as a natural generalisation of the Fourier series to functions defined on infinite domains [3, p. 62]. This subsection provides the conceptual bridge between these two fundamental mathematical tools.

C.1.1 Fourier Series: The Finite Domain Case

As derived in Section 6.2.1, a function $f(x)$ defined on a finite interval $[0, L]$ can be represented as a sum of sine and cosine functions (or equivalently, complex exponentials) [3]:

$$f(x) = \sum_{n=0}^{\infty} c_n e^{ik_n x} \tag{78}$$

where the discrete frequencies are

$$k_n = \frac{2\pi n}{L}, \quad n = 0, \pm 1, \pm 2, \ldots \tag{79}$$

The coefficients are given by

$$c_n = \frac{1}{L} \int_0^L f(x) e^{-ik_n x}\, dx \tag{80}$$

This representation has several key features:

- **Discrete spectrum**: Frequencies come in discrete multiples of the fundamental frequency $2\pi/L$
- **Finite domain**: The function is periodic with period L (or can be extended periodically)
- **Summation**: The representation is a sum over countably many modes

C.1.2 Taking the Limit $L \to \infty$

To extend this representation to functions defined on the entire real line $(-\infty, \infty)$, consider what happens as the domain length L increases without bound.

Frequency spacing becomes infinitesimal: The spacing between adjacent frequencies is

$$\Delta k = k_{n+1} - k_n = \frac{2\pi}{L} \tag{81}$$

As $L \to \infty$, this spacing shrinks to zero: $\Delta k \to 0$. The discrete frequency spectrum becomes continuous.

From sum to integral: In the limit, the discrete sum over frequencies becomes an integral. To see this, rewrite the Fourier series by introducing

$$\Delta k = \frac{2\pi}{L} \quad \Rightarrow \quad \frac{1}{L} = \frac{\Delta k}{2\pi} \tag{82}$$

The Fourier series becomes

$$f(x) = \sum_{n=-\infty}^{\infty} \left[\frac{1}{L} \int_0^L f(\xi) e^{-ik_n \xi} d\xi \right] e^{ik_n x} = \sum_{n=-\infty}^{\infty} \left[\frac{\Delta k}{2\pi} \int_0^L f(\xi) e^{-ik_n \xi} d\xi \right] e^{ik_n x} \tag{83}$$

As $L \to \infty$:

- The integration limits extend to $(-\infty, \infty)$
- The summation becomes a Riemann sum for an integral over the continuous variable k
- The discrete frequencies k_n become a continuous frequency variable k

In the limit, the Fourier series transforms into:

$$f(x) = \frac{1}{2\pi} \int_{-\infty}^{\infty} \left[\int_{-\infty}^{\infty} f(\xi) e^{-ik\xi} d\xi \right] e^{ikx} \, dk \tag{84}$$

The inner integral defines the Fourier transform $\hat{f}(k)$, while the outer integral is the inverse Fourier transform.

C.1.3 Physical Interpretation

This limiting process has a clear physical meaning:

- **Fourier series**: Describes standing waves in a finite cavity (discrete resonant frequencies)
- **Fourier transform**: Describes traveling waves in an unbounded medium (continuous spectrum of frequencies)

For heat diffusion:

- A finite rod supports discrete spatial modes that decay at different rates
- An infinite rod supports a continuous spectrum of wave numbers, each decaying independently

This conceptual framework explains why the Fourier transform is the natural tool for solving the heat equation on infinite or semi-infinite domains, as used in Experiment 2 analysis (Section 6.2.3).

C.2 Definition of the Fourier Transform

The Fourier transform is an integral transform that decomposes a function of space (or time) into its constituent frequencies. For a function $u(x,t)$ defined on the spatial domain $x \in (-\infty, \infty)$, the Fourier transform with respect to x is defined as:

$$\hat{u}(k,t) = \mathcal{F}\{u(x,t)\} = \int_{-\infty}^{\infty} u(x,t)e^{-ikx}\,dx \tag{85}$$

where:

- $\hat{u}(k,t)$ is the Fourier transform of $u(x,t)$
- k is the wavenumber (spatial frequency variable)
- $i = \sqrt{-1}$ is the imaginary unit
- The integration is performed over all space

The Fourier transform maps a function from physical space to frequency space (also called Fourier space or k-space).

C.3 Inverse Fourier Transform

The original function can be recovered from its Fourier transform using the inverse Fourier transform:

$$u(x,t) = \mathcal{F}^{-1}\{\hat{u}(k,t)\} = \frac{1}{2\pi}\int_{-\infty}^{\infty} \hat{u}(k,t)e^{ikx}\,dk \tag{86}$$

The factor of $\frac{1}{2\pi}$ ensures proper normalisation. Note that different conventions exist in the literature: some authors place $(2\pi)^{-1/2}$ in both the forward and inverse transforms, while others place 2π in the forward transform. The convention used here is standard in physics and engineering [3].

C.4 Key Properties of the Fourier Transform

The Fourier transform possesses several properties that make it particularly useful for solving differential equations.

C.4.1 Linearity

For any functions $u(x)$ and $v(x)$ and constants a and b:

$$\mathcal{F}\{a\,u(x) + b\,v(x)\} = a\,\mathcal{F}\{u(x)\} + b\,\mathcal{F}\{v(x)\} \tag{87}$$

This property follows directly from the linearity of integration.

C.4.2 Derivative Property

The Fourier transform of a spatial derivative is:

$$\mathcal{F}\left\{\frac{\partial u}{\partial x}\right\} = ik\,\hat{u}(k) \tag{88}$$

For the second derivative:

$$\mathcal{F}\left\{\frac{\partial^2 u}{\partial x^2}\right\} = -k^2\,\hat{u}(k) \tag{89}$$

Derivation of the Second Derivative Property Starting from the definition of the Fourier transform:

$$\mathcal{F}\left\{\frac{\partial^2 u}{\partial x^2}\right\} = \int_{-\infty}^{\infty} \frac{\partial^2 u}{\partial x^2} e^{-ikx}\,dx$$

Applying integration by parts twice (assuming u and its derivatives vanish at infinity):

First integration by parts:

$$\begin{aligned} &= \left[\frac{\partial u}{\partial x} e^{-ikx}\right]_{-\infty}^{\infty} - \int_{-\infty}^{\infty} \frac{\partial u}{\partial x} \cdot (-ik) e^{-ikx}\,dx \\ &= 0 + ik \int_{-\infty}^{\infty} \frac{\partial u}{\partial x} e^{-ikx}\,dx \end{aligned}$$

Second integration by parts:

$$\begin{aligned} &= ik\left(\left[u e^{-ikx}\right]_{-\infty}^{\infty} - \int_{-\infty}^{\infty} u \cdot (-ik) e^{-ikx}\,dx\right) \\ &= ik\left(0 + ik \int_{-\infty}^{\infty} u e^{-ikx}\,dx\right) \\ &= (ik)^2 \hat{u}(k) = -k^2 \hat{u}(k) \end{aligned}$$

This crucial property converts spatial derivatives into algebraic operations in frequency space, transforming differential equations into algebraic equations.

C.4.3 Convolution Theorem

The Fourier transform of a convolution is the product of the Fourier transforms [3, p. 64]:

$$\mathcal{F}\{u * v\} = \hat{u}(k) \cdot \hat{v}(k) \tag{90}$$

s

where the convolution is defined as:

$$(u * v)(x) = \int_{-\infty}^{\infty} u(\xi) v(x - \xi)\,d\xi \tag{91}$$

This property is fundamental to understanding the solution of the heat equation as a convolution with the heat kernel (Green's function).

C.5 Fourier Transform of a Gaussian

A particularly important result for Experiment 2 is that the Fourier transform of a Gaussian function is also a Gaussian. For:

$$u(x) = A \exp\left(-\frac{x^2}{2\sigma^2}\right) \tag{92}$$

the Fourier transform is:

$$\hat{u}(k) = A\sigma\sqrt{2\pi} \exp\left(-\frac{\sigma^2 k^2}{2}\right), \tag{93}$$

as derived in Section 6.2.3. This self-similarity property of Gaussians under Fourier transformation is essential for the analytical solution of Experiment 2.

C.6 Application to the Heat Equation

When the Fourier transform is applied to the one-dimensional heat equation:

$$\frac{\partial u}{\partial t} = \alpha \frac{\partial^2 u}{\partial x^2}$$

using the derivative property (89), it becomes:

$$\frac{\partial \hat{u}}{\partial t} = -\alpha k^2 \hat{u} \tag{94}$$

This is a first-order ordinary differential equation in time for each mode k, which can be solved by separation of variables to give:

$$\hat{u}(k,t) = \hat{u}(k,0) e^{-\alpha k^2 t} \tag{95}$$

The solution in physical space is then recovered by inverse Fourier transform, as derived in Section 6.2.3.

C.7 Numerical Implementation: The Fast Fourier Transform

The discrete Fourier transform (DFT) approximates the continuous Fourier transform for sampled data. For N equally-spaced samples $u_j = u(x_j)$ where $x_j = j\Delta x$ and $j = 0, 1, \ldots, N-1$, the DFT is:

$$\hat{u}_n = \sum_{j=0}^{N-1} u_j e^{-2\pi i j n/N} \tag{96}$$

The Fast Fourier Transform (FFT) is an algorithm that computes the DFT in $\mathcal{O}(N \log N)$ operations rather than the $\mathcal{O}(N^2)$ operations required by the direct summation [3]. This computational efficiency makes spectral methods practical for solving partial differential equations, as implemented in the simulation section.

D Derivation of the Forward Euler Scheme

(Adapted from [23])

This appendix presents the detailed derivation of the Forward Euler (FTCS) finite difference scheme for the one-dimensional heat equation, as referenced in Section 6.4.

D.1 Taylor Series Expansion

The derivation begins with Taylor series expansions of the temperature function $u(x,t)$ about a point (x,t) in both space and time.

D.1.1 Temporal Derivative Approximation

Expanding $u(x,t+\Delta t)$ in a Taylor series about time t:

$$u(x,t+\Delta t) = u(x,t) + \frac{\partial u}{\partial t}\Delta t + \frac{\partial^2 u}{\partial t^2}\frac{(\Delta t)^2}{2!} + \mathcal{O}((\Delta t)^3) \tag{97}$$

Rearranging to isolate the first-order time derivative:

$$\frac{\partial u}{\partial t} = \frac{u(x,t+\Delta t) - u(x,t)}{\Delta t} + \mathcal{O}(\Delta t) \tag{98}$$

This is the *forward difference* approximation for the time derivative, accurate to first order in Δt.

D.1.2 Spatial Second Derivative Approximation

For the spatial second derivative, two Taylor expansions are needed. First, expanding $u(x+\Delta x,t)$ forward in space:

$$u(x+\Delta x,t) = u(x,t) + \frac{\partial u}{\partial x}\Delta x + \frac{\partial^2 u}{\partial x^2}\frac{(\Delta x)^2}{2!} + \frac{\partial^3 u}{\partial x^3}\frac{(\Delta x)^3}{3!} + \mathcal{O}((\Delta x)^4) \tag{99}$$

Then, expanding $u(x-\Delta x,t)$ backward in space:

$$u(x-\Delta x,t) = u(x,t) - \frac{\partial u}{\partial x}\Delta x + \frac{\partial^2 u}{\partial x^2}\frac{(\Delta x)^2}{2!} - \frac{\partial^3 u}{\partial x^3}\frac{(\Delta x)^3}{3!} + \mathcal{O}((\Delta x)^4) \tag{100}$$

Adding these two expansions:

$$u(x+\Delta x,t) + u(x-\Delta x,t) = 2u(x,t) + \frac{\partial^2 u}{\partial x^2}(\Delta x)^2 + \mathcal{O}((\Delta x)^4)$$

Note that the first and third derivative terms cancel due to symmetry. Solving for the second derivative:

$$\frac{\partial^2 u}{\partial x^2} = \frac{u(x+\Delta x,t) - 2u(x,t) + u(x-\Delta x,t)}{(\Delta x)^2} + \mathcal{O}((\Delta x)^2) \tag{101}$$

This is the *centred difference* approximation for the spatial second derivative, accurate to second order in Δx.

D.2 Discretisation

Introducing the discrete notation:

$$x_i = i\Delta x, \quad i = 0,1,2,\ldots,N-1 \tag{102}$$

$$t_n = n\Delta t, \quad n = 0,1,2,\ldots \tag{103}$$

$$u_i^n \approx u(x_i,t_n) \tag{104}$$

The finite difference approximations become:

$$\left.\frac{\partial u}{\partial t}\right|_i^n \approx \frac{u_i^{n+1} - u_i^n}{\Delta t} \tag{105}$$

$$\left.\frac{\partial^2 u}{\partial x^2}\right|_i^n \approx \frac{u_{i+1}^n - 2u_i^n + u_{i-1}^n}{(\Delta x)^2} \tag{106}$$

D.3 Substitution into the Heat Equation

The one-dimensional heat equation is:

$$\frac{\partial u}{\partial t} = \alpha \frac{\partial^2 u}{\partial x^2} \tag{107}$$

Substituting the finite difference approximations:

$$\frac{u_i^{n+1} - u_i^n}{\Delta t} = \alpha \frac{u_{i+1}^n - 2u_i^n + u_{i-1}^n}{(\Delta x)^2} \tag{108}$$

D.4 Explicit Update Formula

Multiplying both sides by Δt and rearranging to solve for u_i^{n+1}:

$$u_i^{n+1} - u_i^n = \alpha \frac{\Delta t}{(\Delta x)^2} \left(u_{i+1}^n - 2u_i^n + u_{i-1}^n\right) \tag{109}$$

$$u_i^{n+1} = u_i^n + \alpha \frac{\Delta t}{(\Delta x)^2} \left(u_{i+1}^n - 2u_i^n + u_{i-1}^n\right) \tag{110}$$

Defining the dimensionless parameter (mesh Fourier number):

$$r = \frac{\alpha \Delta t}{(\Delta x)^2} \tag{111}$$

The final explicit update formula is:

$$\boxed{u_i^{n+1} = u_i^n + r\left(u_{i+1}^n - 2u_i^n + u_{i-1}^n\right)} \tag{112}$$

This can also be written in expanded form:

$$\boxed{u_i^{n+1} = (1-2r)u_i^n + r\,u_{i+1}^n + r\,u_{i-1}^n} \tag{113}$$

D.5 Stability Analysis

[21]

The stability of the Forward Euler scheme can be analyzed using von Neumann stability analysis. Assuming a Fourier mode of the form:

$$u_i^n = \xi^n e^{ikx_i} \tag{114}$$

where ξ is the amplification factor and k is the wavenumber. Substituting into the update formula:

$$\xi^{n+1}e^{ikx_i} = (1-2r)\xi^n e^{ikx_i} + r\xi^n e^{ik(x_i+\Delta x)} + r\xi^n e^{ik(x_i-\Delta x)}$$

Dividing by $\xi^n e^{ikx_i}$:

$$\xi = 1 - 2r + re^{ik\Delta x} + re^{-ik\Delta x}$$

Using Euler's formula $e^{i\theta} + e^{-i\theta} = 2\cos\theta$:

$$\xi = 1 - 2r + 2r\cos(k\Delta x) = 1 - 2r(1 - \cos(k\Delta x))$$

Using the trigonometric identity $1 - \cos\theta = 2\sin^2(\theta/2)$:

$$\xi = 1 - 4r\sin^2\left(\frac{k\Delta x}{2}\right)$$

For stability, $|\xi| \leq 1$ for all wavenumbers k is required. The worst case occurs when $\sin^2(k\Delta x/2) = 1$ (highest frequency modes):

$$-1 \leq 1 - 4r \leq 1 \tag{115}$$

The left inequality gives $4r \leq 2$, which yields the CFL stability condition:

$$\boxed{r = \frac{\alpha\Delta t}{(\Delta x)^2} \leq \frac{1}{2}} \tag{116}$$

This is the necessary and sufficient condition for stability of the Forward Euler scheme for the heat equation.

E Source Code Listings

This appendix contains the complete, documented source code for the Manim simulations presented in Section 7. All code is written in Python 3.8+ and uses the Manim Community Edition library for visualisation. The code has been extensively commented to explain both the mathematical algorithms and their Python implementation.

E.1 Mixed Boundary Conditions: Forward Euler Method

The following script simulates Experiment 1 (continuous heating at one end) using explicit finite differences:

```
from manim import *
import numpy as np

def second_derivative_space(u, dx):
    # Compute second spatial derivative using centered finite differences.
    return (u[2:] - 2 * u[1:-1] + u[:-2]) / dx**2


class HeatEquationMixedBCs_Euler(Scene):
    def construct(self):
```

```
# PHYSICAL PARAMETERS

L = 0.3                     # Rod length [m]
alpha = 1.9e-4              # Thermal diffusivity [m²/s]
T_source = 110.0            # Boundary temperature at x=0 [°C]


# NUMERICAL PARAMETERS

N = 100                     # Number of spatial grid points
x = np.linspace(0, L, N)    # Spatial grid
dx = x[1] - x[0]            # Grid spacing

# Time step chosen to satisfy CFL stability condition
dt = 0.005                  # Time step [s]
r = alpha * dt / dx**2      # Diffusion number (mesh Fourier number)


# Total simulation parameters
t_max = 300.0               # Total simulation time [s]
n_steps = int(t_max / dt)   # Number of time steps

# Frame skip for animation (show every Nth frame)
frame_skip = max(1, n_steps // 500)


# VISUALISATION SETUP


axes = Axes(
    x_range=[0, 0.3, 0.05],
    y_range=[20, 120, 20],
    x_length=10,
    y_length=5,
    axis_config={"include_numbers": True, "font_size": 24},
    tips=False,
).center()

y_label = (
    Text("Temperature [°C]", font_size=30)
    .rotate(PI / 2)
    .next_to(axes.y_axis, LEFT, buff=0.6)
)

x_label = axes.get_x_axis_label(
    "Position [m]",
    edge=DOWN,
    direction=DOWN
)

labels = VGroup(y_label, x_label)
```

```
self.play(Create(axes), Create(labels))


# INITIAL CONDITION (Experiment~1 data)


# Experimental measurement positions and temperatures
x_data = np.array([0.01, 0.043, 0.086, 0.129, 0.171, 0.214, 0.257, 0.300])
u_data = np.array([22.2, 22.1, 22.0, 22.0, 22.0, 22.0, 22.5, 22.5])

# Interpolate to computational grid and scale positions to [0, L]
u = np.interp(x, x_data * (L / x_data[-1]), u_data)

# Store initial state
u_history = [u.copy()]


# TIME STEPPING (Forward Euler Method)



for step in range(n_steps):
    # Compute second derivative at interior points
    d2u = second_derivative_space(u, dx)

    # Update interior points using Forward Euler formula
    u[1:-1] += alpha * dt * d2u

    # Apply boundary conditions:
    # Left (x=0): Dirichlet BC - fixed temperature
    u[0] = T_source

    # Right (x=L): Neumann BC - zero flux (insulated)
    # Approximated as u[N-1] = u[N-2] (zero gradient)
    u[-1] = u[-2]

    # Store frame for animation
    if step % frame_skip == 0:
        u_history.append(u.copy())



# ANIMATION SETUP


# Value tracker for frame index
frame_tracker = ValueTracker(0)

# Animated temperature curve
curve = always_redraw(
```

```
            lambda: axes.plot_line_graph(
                x_values=x,
                y_values=u_history[int(frame_tracker.get_value())],
                add_vertex_dots=False,
                line_color=RED,
            )
        )

        # Time display
        time_text = always_redraw(
            lambda: Text(
                f"t = {int(int(frame_tracker.get_value()) * frame_skip * dt)} s",
                font_size=30
            ).to_edge(UP).shift(DOWN*0.5)
        )


        # ANIMATION


        self.add(curve, time_text)
        self.wait(1)

        # Animate through all stored frames
        self.play(
            frame_tracker.animate.set_value(len(u_history) - 1),
            run_time=8,
            rate_func=linear
        )

        self.wait(2)
```

E.2 Neumann Boundary Conditions: Forward Euler Method

This script simulates an idealised version of Experiment 2 (diffusion of a Gaussian peak) using explicit finite differences:

```
from manim import *
import numpy as np

def second_derivative_space(u, dx):
    """
    Compute second spatial derivative using centered finite differences.

    Uses the three-point stencil:
        d²u/dx² = (u[i+1] - 2u[i] + u[i-1]) / dx²

    Parameters:
        u (array): Temperature array at current time
        dx (float): Spatial grid spacing
```

```
    Returns:
        array: Second derivative at interior points [1:-1]
    """
    return (u[2:] - 2 * u[1:-1] + u[:-2]) / dx**2


class HeatEquationNeumann_Euler(Scene):
    def construct(self):

        # PHYSICAL PARAMETERS


        L = 0.3                     # Rod length [m]
        alpha = 1.9e-4              # Thermal diffusivity [m²/s]
        T_ambient = 22.0            # Ambient/background temperature [°C]


        # NUMERICAL PARAMETERS


        N = 100                     # Number of spatial grid points
        x = np.linspace(0, L, N)    # Spatial grid
        dx = x[1] - x[0]            # Grid spacing

        # Time step chosen to satisfy CFL stability condition
        dt = 0.005                  # Time step [s]
        r = alpha * dt / dx**2      # Diffusion number


        # Total simulation parameters
        t_max = 120.0               # Total simulation time [s]
        n_steps = int(t_max / dt)   # Number of time steps

        # Frame skip for animation
        frame_skip = max(1, n_steps // 500)


        # VISUALISATION SETUP


        axes = Axes(
            x_range=[0, 0.3, 0.05],
            y_range=[20, 35, 5],
            x_length=10,
            y_length=5,
            axis_config={"include_numbers": True, "font_size": 24},
            tips=False,
        ).center()

        y_label = (
```

```
    Text("Temperature [°C]", font_size=30)
    .rotate(PI / 2)
    .next_to(axes.y_axis, LEFT, buff=0.6)
)

x_label = axes.get_x_axis_label(
    "Position [m]",
    edge=DOWN,
    direction=DOWN
)

labels = VGroup(y_label, x_label)

self.play(Create(axes), Create(labels))


# INITIAL CONDITION (Gaussian temperature peak)


# Experimental measurement positions and temperatures
x_data = np.array([0.01, 0.043, 0.086, 0.129, 0.171, 0.214, 0.257, 0.300])
u_data = np.array([26.0, 27.2, 29.8, 33.2, 33.5, 30.0, 26.4, 25.8])

# Interpolate to computational grid
u = np.interp(x, x_data, u_data)

# Store initial state
u_history = [u.copy()]


# TIME STEPPING (Forward Euler Method)


for step in range(n_steps):
    # Compute second derivative at interior points
    d2u = second_derivative_space(u, dx)

    # Update interior points using Forward Euler formula
    u[1:-1] += alpha * dt * d2u

    # Apply Neumann boundary conditions at both ends:
    # Zero flux approximated as zero gradient

    # Left boundary (x=0)
    u[0] = u[1]

    # Right boundary (x=L)
    u[-1] = u[-2]

    # Store frame for animation
    if step % frame_skip == 0:
```

```
        u_history.append(u.copy())


# Verify energy conservation
initial_energy = np.sum(u_history[0])
final_energy = np.sum(u_history[-1])
energy_change = abs(final_energy - initial_energy) / initial_energy * 100


# ANIMATION SETUP


# Value tracker for frame index
frame_tracker = ValueTracker(0)

# Animated temperature curve
curve = always_redraw(
    lambda: axes.plot_line_graph(
        x_values=x,
        y_values=u_history[int(frame_tracker.get_value())],
        add_vertex_dots=False,
        line_color=BLUE,
    )
)

# Time display
time_text = always_redraw(
    lambda: Text(
        f"t = {int(int(frame_tracker.get_value()) * frame_skip * dt)} s",
        font_size=30
    ).to_edge(UP).shift(DOWN*0.5)
)


# ANIMATION


self.add(curve, time_text)
self.wait(1)

# Animate through all stored frames
self.play(
    frame_tracker.animate.set_value(len(u_history) - 1),
    run_time=8,
    rate_func=linear
)

self.wait(2)
```

E.3 Spectral Method: Fast Fourier Transform

This script simulates Experiment 2 using the FFT spectral method, demonstrating the efficiency advantages of frequency-space computation:

```
from manim import *
import numpy as np

class HeatEquation_FFT(Scene):
    def construct(self):

        # PHYSICAL AND NUMERICAL PARAMETERS


        # Physical parameters
        L = 0.3              # Rod length [m]
        alpha = 1.9e-4       # Thermal diffusivity [m²/s]
        t_max = 120          # Total simulation time [s]

        # Numerical parameters
        N = 256              # Grid points (power of 2 for FFT efficiency)
        dt = 1.0             # Time step [s]


        # SPATIAL GRID SETUP


        # Create uniform spatial grid
        dx = L / (N - 1)     # Grid spacing (N-1 for endpoint=True)
        x = np.linspace(0, L, N, endpoint=True)



        # INITIAL CONDITION (Experiment˜2 data)


        # Experimental measurement positions and temperatures
        x_data = np.array([0.01, 0.043, 0.086, 0.129, 0.171, 0.214, 0.257, 0.300])
        u_data = np.array([26.0, 27.2, 29.8, 33.2, 33.5, 30.0, 26.4, 25.8])

        # Interpolate to computational grid
        u0 = np.interp(x, x_data, u_data)



        # FFT SPECTRAL METHOD SETUP


        # Transform initial condition to frequency space
        u_hat0 = np.fft.fft(u0)

        # Compute frequency array for periodic domain [0, L]
```

```
# FFT frequencies: k_n = 2*pi*n / L for n = 0, 1, ..., N-1
k = 2 * np.pi * np.fft.fftfreq(N, d=dx)



# VISUALISATION SETUP


# Create coordinate axes
axes = Axes(
    x_range=[0, 0.3, 0.05],      # Position axis: 0 to 0.3 m
    y_range=[25, 35, 5],         # Temperature axis: 25 to 35 °C
    x_length=10,                 # Visual width
    y_length=5,                  # Visual height
    axis_config={"include_numbers": True, "font_size": 24},
    tips=False,
).center()

# Axis labels
y_label = (
    Text("Temperature [°C]", font_size=30)
    .rotate(PI / 2)
    .next_to(axes.y_axis, LEFT, buff=0.6)
)

x_label = axes.get_x_axis_label(
    "Position [m]",
    edge=DOWN,
    direction=DOWN
)

labels = VGroup(y_label, x_label)

# Display axes and labels
self.play(Create(axes), Create(labels))


# TIME EVOLUTION


# Value tracker for animation time
time_tracker = ValueTracker(0)

def solution():
    """
    Compute temperature distribution at current time.

    The solution in frequency space is:
        û(k,t) = û(k,0) exp(-alpha*k²t)

    Each Fourier mode decays exponentially at rate alpha*k².
```

```
        Higher frequencies (fine spatial features) decay faster.
        """
        t = time_tracker.get_value()

        # Apply exponential decay to each Fourier mode
        u_hat_t = u_hat0 * np.exp(-alpha * k**2 * t)

        # Transform back to physical space
        u_t = np.real(np.fft.ifft(u_hat_t))

        return u_t

    # Create animated temperature profile
    graph = always_redraw(
        lambda: axes.plot_line_graph(
            x_values=x,
            y_values=solution(),
            add_vertex_dots=False,
            line_color=BLUE,
            stroke_width=3,
        )
    )

    # Time display
    time_label = always_redraw(
        lambda: Text(
            f"t = {int(time_tracker.get_value())} s",
            font_size=30
        ).to_edge(UP).shift(DOWN*0.5)
    )


    # ANIMATION


    # Add graph and time label to scene
    self.add(graph, time_label)
    self.wait(1)

    # Animate time evolution from t=0 to t=t_max
    self.play(
        time_tracker.animate.set_value(t_max),
        run_time=8,
        rate_func=linear
    )

    self.wait(2)
```

E.4 Shared Helper Functions

The two scripts using Forward Euler method have the following shared structure:

E.4.1 Second Derivative Computation

The `second_derivative_space()` function computes the centred finite difference approximation:

```
def second_derivative_space(u, dx):
    return (u[2:] - 2 * u[1:-1] + u[:-2]) / dx**2
```

This three-point stencil is second-order accurate in space and forms the core of the Forward Euler method.

E.4.2 Boundary Condition Implementation

Dirichlet (fixed temperature):

```
u[0] = T_source  # Fix temperature at boundary
```

Neumann (zero flux):

```
u[0] = u[1]      # Zero gradient
u[-1] = u[-2]    # Symmetric at both ends
```

E.5 Execution Instructions

Environment Setup Install required packages:

```
pip install manim numpy matplotlib
```

Running the Simulations Execute each script using the Manim CLI:

```
# High quality rendering
manim -pqh HeatEquationMixedBCs_Euler.py HeatEquationMixedBCs_Euler
manim -pqh HeatEquationNeumann_Euler.py HeatEquationNeumann_Euler
manim -pqh HeatEquation_FFT.py HeatEquation_FFT

# Fast preview (low quality)
manim -pql [filename] [SceneName]
```

The `-p` flag automatically plays the animation after rendering, `-q` sets quality (`l`=low, `m`=medium, `h`=high), and the final argument specifies the Scene class to render.

Computational Requirements Rendering times on a typical modern computer:

- Forward Euler simulations: 2–5 minutes at high quality
- FFT simulation: 1–2 minutes at high quality
- Memory usage: < 1 GB for all simulations

The high computational cost for Forward Euler reflects the large number of time steps (24,000–60,000) required to maintain stability, whereas the FFT method requires only 120 steps.

E.6 Notes on Numerical Precision

All floating-point computations use NumPy's default `float64` (double precision), providing approximately 15 decimal digits of precision. The main sources of numerical error are:

1. **Truncation error**: Forward Euler is $\mathcal{O}(\Delta t)$ in time, $\mathcal{O}(\Delta x^2)$ in space
2. **Round-off error**: Accumulates over many time steps in Forward Euler
3. **Aliasing**: Can occur in FFT if the solution develops high-frequency components

For the parameters chosen in these simulations, truncation error dominates round-off error, and the solutions are sufficiently smooth to avoid aliasing issues.

List of Figures

References

[1] Grant Sanderson. 3blue1brown YouTube channel. https://www.youtube.com/c/3blue1brown. access: 01.02.2025.

[2] Jiří Lebl. *Notes on Diffy Qs: Differential Equations for Engineers*. University of Victoria, 2014.

[3] Steven L. Brunton and J. Nathan Kutz. *Data-Driven Science and Engineering*. Cambridge University Press, 2022.

[4] Steven L. Brunton. Eigensteve YouTube channel. https://www.youtube.com/@Eigensteve. access: 19.07.2025.

[5] Tom Crawford. Tom rocks maths YouTube channel. https://www.youtube.com/@TomRocksMaths. access: 19.07.2025.

[6] Wikipedia contributors. Thermodynamics. https://en.wikipedia.org/wiki/Thermodynamics. access: 08.12.2025.

[7] H. A. Buchdahl. *The Concepts of Classical Thermodynamics*. Cambridge University Press, 1966.

[8] Wikipedia contributors. Thermal equilibrium. https://en.wikipedia.org/wiki/Thermalequilibrium. access: 08.12.2025.

[9] Wikipedia contributors. First law of thermodynamics. https://en.wikipedia.org/wiki/First_law_of_thermodynamics. access: 13.12.2025.

[10] Wikipedia contributors. Thermal conduction. https://en.wikipedia.org/wiki/Thermal_conduction#Fourier's_law. access: 18.12.2025.

[11] Wikipedia contributors. Newton's law of cooling. https://en.wikipedia.org/wiki/Newton%27s_law_of_cooling. access: 18.12.2025.

[12] D.G. Zill. *A First Course in Differential Equations with Modeling Applications*. Cengage Learning, 2012.

[13] T. N. Narasimhan. *Fourier's Heat Conduction Equation: History, Influence, and Connections*. AGU Publications, 1999.

[14] IndMALL contributors. What is the role of hysteresis in temperature control? https://www.indmall.in/faq/what-is-the-role-of-hysteresis-in-temperature-control/. access: 23.12.2025.

[15] Wikipedia contributors. Thermal diffusivity. https://en.wikipedia.org/wiki/Thermal_diffusivity. access: 24.12.2025.

[16] Anderson. Fluids – lecture 6 notes. https://web.mit.edu/16.unified/www/FALL/fluids/Lectures/f06.pdf. access: 25.12.2025.

[17] Yue-Xian Li. Math 215/255 lecture notes 2019. https://personal.math.ubc.ca/~yxli/m215-255/m255_notes_2019.pdf. access: 28.12.2025.

[18] Y. D. Chong. 3.5: The gaussian integral. https://phys.libretexts.org/Bookshelves/Mathematical_Physics_and_Pedagogy/Complex_Methods_for_the_Sciences_(Chong)/03%3A_Integrals/3.05%3A_The_Gaussian_Integral#. access: 28.12.2025.

[19] Kurt Bryan. Green's functions and the heat equation. https://www.rose-hulman.edu/~bryan/lottamath/heatkern.pdf. access: 28.12.2025.

[20] Taylor & Francis contributers. Fourier number. https://taylorandfrancis.com/knowledge/Engineering_and_technology/Industrial_engineering_%26_manufacturing/Fourier_number/#. access: 27.12.2025.

[21] R. R. Rosales. Notes: von neumann stability analysis. https://math.mit.edu/classes/18.300/Notes/Notes_vNSA.pdf. access: 27.12.2025.

[22] James W. Cooley and John W. Tukey. An algorithm for the machine calculation of complex fourier series. *Mathematics of Computation*, 1965.

[23] Steve L. Brunton. Error analysis of euler integration scheme for differential equations using taylor series. https://www.youtube.com/watch?v=h2i550iaEv0. access: 19.07.2025.

Plagiarism Declaration

Ich bestätige hiermit, dass ich meine Maturaarbeit selbstständig und ohne unerlaubte Mithilfe verfasst und keine anderen als die angegebenen Quellen benutzt habe. Alle Stellen, die wörtlich oder sinngemäss aus Quellen entnommen wurden, habe ich als solche gekennzeichnet. Teile, die mit erlaubter Hilfe entstanden sind, habe ich klar deklariert.

Olten, 01.01.2026

Suvirr Malli